JVI Journals.ASM.org

Characterization of the Mode of Action of a Potent Dengue Virus Capsid Inhibitor

Pietro Scaturro,[a] Iuni Margaret Laura Trist,[b] David Paul,[a] Anil Kumar,[a]* Eliana G. Acosta,[a] Chelsea M. Byrd,[c]* Robert Jordan,[c]* Andrea Brancale,[b] Ralf Bartenschlager[a,d]

Department of Infectious Diseases, Molecular Virology, Heidelberg University, Heidelberg, Germany[a]; School of Pharmacy and Pharmaceutical Sciences, Cardiff University, Cardiff, United Kingdom[b]; SIGA Technologies, Inc., Corvallis, Oregon, USA[c]; German Center for Infection Research, Heidelberg, Germany[d]

ABSTRACT

Dengue viruses (DV) represent a significant global health burden, with up to 400 million infections every year and around 500,000 infected individuals developing life-threatening disease. In spite of attempts to develop vaccine candidates and antiviral drugs, there is a lack of approved therapeutics for the treatment of DV infection. We have previously reported the identification of ST-148, a small-molecule inhibitor exhibiting broad and potent antiviral activity against DV *in vitro* and *in vivo* (C. M. Byrd et al., Antimicrob. Agents Chemother. 57:15–25, 2013, doi:10.1128/AAC.01429-12). In the present study, we investigated the mode of action of this promising compound by using a combination of biochemical, virological, and imaging-based techniques. We confirmed that ST-148 targets the capsid protein and obtained evidence of bimodal antiviral activity affecting both assembly/release and entry of infectious DV particles. Importantly, by using a robust bioluminescence resonance energy transfer-based assay, we observed an ST-148-dependent increase of capsid self-interaction. These results were corroborated by molecular modeling studies that also revealed a plausible model for compound binding to capsid protein and inhibition by a distinct resistance mutation. These results suggest that ST-148-enhanced capsid protein self-interaction perturbs assembly and disassembly of DV nucleocapsids, probably by inducing structural rigidity. Thus, as previously reported for other enveloped viruses, stabilization of capsid protein structure is an attractive therapeutic concept that also is applicable to flaviviruses.

IMPORTANCE

Dengue viruses are arthropod-borne viruses representing a significant global health burden. They infect up to 400 million people and are endemic to subtropical and tropical areas of the world. Currently, there are neither vaccines nor approved therapeutics for the prophylaxis or treatment of DV infections, respectively. This study reports the characterization of the mode of action of ST-148, a small-molecule capsid inhibitor with potent antiviral activity against all DV serotypes. Our results demonstrate that ST-148 stabilizes capsid protein self-interaction, thereby likely perturbing assembly and disassembly of viral nucleocapsids by inducing structural rigidity. This, in turn, might interfere with the release of viral RNA from incoming nucleocapsids (uncoating) as well as assembly of progeny virus particles. As previously reported for other enveloped viruses, we propose the capsid as a novel tractable target for flavivirus inhibitors.

Dengue virus (DV) belongs to the genus *Flavivirus*, a large group of emerging pathogens capable of causing severe human diseases. Among these, DV represents the most prevalent mosquito-borne human-pathogenic virus worldwide, comprising 4 serotypes that are transmitted mainly by infected *Aedes* mosquitoes during a blood meal. DV infections can lead to a wide range of clinical manifestations, ranging from asymptomatic infections to life-threatening dengue hemorrhagic fever and shock syndrome. A recent study estimated around 390 million DV infections each year, resulting in approximately 100 million symptomatic cases and around 25,000 deaths (1). Despite intense efforts and growing public interest, no licensed antiviral drug against DV infection is available, and the most advanced DV vaccine candidate did not meet expectations in a recent large clinical trial (2).

DV has a single-stranded RNA genome of positive polarity that codes for a polyprotein, which is co- and posttranslationally processed into three structural proteins (capsid, prM, and envelope) and seven nonstructural proteins (NS1, NS2A, NS2B, NS3, NS4A, NS4B, and NS5) (3). The virus enters mammalian cells via receptor-mediated endocytosis. In the endosomal compartment, the low pH induces a conformational change in the envelope (E) protein, triggering membrane fusion and nucleocapsid release into the cytoplasm (4, 5). Disassembly of the nucleocapsid occurs by a poorly understood mechanism leading to the release of viral RNA into the cytoplasm of infected cells. Upon synthesis of viral proteins, massive intracellular membrane remodeling events occur, which is a conserved feature among plus-strand RNA viruses (6, 7). These rearrangements include membrane invaginations into the endoplasmic reticulum (ER), which are the assumed sites of

Received 17 June 2014 **Accepted** 18 July 2014

Published ahead of print 23 July 2014

Editor: M. S. Diamond

Address correspondence to Ralf Bartenschlager, ralf.bartenschlager@med.uni-heidelberg.de.

* Present address: Anil Kumar, Department of Cell Biology, Faculty of Medicine and Dentistry, University of Alberta, Edmonton, Alberta, Canada; Chelsea M. Byrd, Kineta, Inc., Seattle, Washington, USA; Robert Jordan, Gilead Sciences, Inc., Foster City, California, USA.

Supplemental material for this article may be found at http://dx.doi.org/10.1128/JVI.01745-14.

doi:10.1128/JVI.01745-14

flavivirus genome replication, and can be observed in both mammalian and arthropod cells (8, 9). Nucleocapsid formation is thought to occur in close proximity to replication sites (9). The envelope is acquired by budding through the ER membrane into which the envelope proteins E and prM have been inserted. Assembled virions, stored within ER stacks in highly ordered arrays, are released from the cell via the conventional secretory pathway, where cleavage of the prM protein by furin, a protease residing in the *trans*-Golgi network (TGN), occurs. This cleavage is required to render DV particles infectious.

The mature capsid protein (C) is a highly basic protein of 12 kDa that forms homodimers in solution (10, 11). The three-dimensional structure of DV C protein was solved by nuclear magnetic resonance (NMR) (12), indicating that the monomer consists of four alpha helices (α1 to α4). The longest helix, α4, extends away from the core of the protein. It has a high density of basic amino acid residues on the solvent-accessible surface that were proposed to interact with the viral RNA. On the opposite side of the molecule, the surface, formed primarily by α2-α2′ and α1-α1′, is largely uncharged and proposed to interact with membranes (12). Although the C protein is the least conserved among flavivirus proteins, both its charge distribution and structural properties are well conserved.

We have recently reported the identification of a small-molecule inhibitor, ST-148, inhibiting replication of all DV serotypes with high potency (13). Intraperitoneal and intravenous administrations of ST-148 in the AG129 mouse model revealed good bioavailability of the compound, which significantly reduced plasma viremia and viral load in spleen and liver of DV-infected mice. Selection of ST-148-resistant viruses led to the identification of a single S34L amino acid change in C protein which was shown to confer resistance to ST-148. Additionally, *in vitro* binding studies of ST-148 to purified C protein suggested that the compound bound equally well to wild-type (WT) and S34L-containing C proteins. Although these studies identified C protein as the primary target of ST-148, its mode of action remained unknown. In the present study, we addressed this aspect by using a combination of biochemical, virological, and imaging-based methods. We obtained evidence that ST-148 enhanced C protein self-interaction, providing an explanation for the observed impairment of DV assembly/release as well as entry competence of virus particles.

MATERIALS AND METHODS

Antibodies and sera. Mouse monoclonal antibodies recognizing human glyceraldehyde-3-phosphate dehydrogenase (GAPDH) (sc-47724/0411) and human lamin A/C (sc-7292/636) were purchased from Santa Cruz Biotechnology (Santa Cruz, CA). Mouse monoclonal antibody against human ATP5B (3D5; no. ab14730) was purchased from Abcam, and mouse monoclonal antibody against human vimentin (VI-10) was obtained from GeneTex Inc. (Irvine, CA). Mouse anti-Envelope monoclonal antibody (3H5-1) was purchased from the ATCC. Mouse anti-capsid monoclonal antibody derived from hybridoma cells (6F3.1) was a kind gift of John G. Aaskov (Queensland University of Technology, Australia), and rabbit polyclonal serum anti-capsid was a kind gift of Andrea Gamarnik (Fundación Instituto Leloir, Argentina). J2 mouse monoclonal anti-double-stranded RNA (dsRNA) antibody was purchased from English and Scientific Consulting (Szirak, Hungary). The secondary anti-mouse and anti-rabbit horseradish peroxidase-conjugated antibodies were purchased from Sigma-Aldrich (St. Louis, MO).

BRET. For donor saturation assays (DSA), 293T cells were transfected in 24-well plates with 20 ng/well of the DNA construct coding for the bioluminescence resonance energy transfer (BRET) donor (Rluc-capsid) and increasing amounts (20 to 1,000 ng/well) of the DNA construct coding for the BRET acceptor (yellow fluorescent protein [YFP] capsid). The total amount of transfected DNA was completed to 1,020 ng with pcDNA 3.1(+) empty vector. Forty-eight hours after transfection, cells were washed with phosphate-buffered saline (PBS) and harvested in 290 μl PBS. For each sample, three aliquots of 90 μl were distributed to wells of a 96-well microplate (black, flat bottomed; Nalgene Nunc, New York, NY). Total YFP expression was measured by using a Mithras LB940 plate reader (Berthold Technologies, Bad Wildbad, Germany), with excitation and emission filters set at 485 and 535 nm, respectively. The luciferase substrate coelenterazine H (PJK, Kleinblittersdorf, Germany) then was added to a final concentration of 5 μM, and luminescence and fluorescence emissions were measured consecutively using a Mithras LB940 plate reader. For BRET measurements, filters were set to 485 nm for luciferase emission and 535 nm for YFP emission. Donor saturation curves were obtained by plotting the BRET values on the *y* axis and the ratio between the fluorescence of the acceptor (netYFP = YFP − YFP_0, where YFP_0 is the fluorescence value in cells expressing the BRET donor alone) and the luminescence of the donor on the *x* axis. For ST-148 dose-response curves, a 1:50 ratio of donor to acceptor (in the $BRET_{max}$ range) was used, and various concentrations of ST-148 (10, 5, 2.5, 1.25, 0.625, 0.312, 0.156, 0.078, 0.039, 0.019, 0.0097, and 0.0048 μM), or the highest equivalent amount of dimethylsulfoxide (DMSO) solute, were added to each well 30 min before transfection. BRET ratios were calculated as described by Angers et al. (14).

Cell culture. Huh7, VeroE6, BHK-21, and HEK-293T cells were maintained in Dulbecco's modified Eagle medium (DMEM; Invitrogen, Karlsruhe, Germany) supplemented with 2 mM L-glutamine, nonessential amino acids, 100 U of penicillin/ml, 100 μg of streptomycin/ml, and 10% fetal calf serum. Cells were passaged in regular intervals by trypsinization and replating of appropriate dilutions.

Immunoblot analysis. Samples were denatured in 2× protein sample buffer (200 mM Tris [pH 8.8], 5 mM EDTA, 0.1% bromophenol blue, 10% sucrose, 3% SDS, 1 mM dithiothreitol [DTT]) and incubated for 5 min at 95°C. Proteins were separated by SDS-PAGE and transferred onto polyvinylidene difluoride membranes by using a mini-SDS-PAGE wet-blotting apparatus (Bio-Rad, Munich, Germany). Membranes were blocked with 5% nonfat dry milk in PBS-0.5% Tween 20 (PBST) and incubated with primary antibodies (capsid, 1:50; GAPDH, 1:1,000; lamin A/C 1:1,000; vimentin, 1:1,000; ATP5B, 1:1,000) by overnight incubation at 4°C. After 3 washes with PBST, membranes were incubated with secondary horseradish peroxidase-conjugated antibodies, developed with the Western lightning plus-ECL reagent (PerkinElmer, Waltham, MA), and bands were imaged using an Intas ChemoCam Imager 3.2 (Intas, Göttingen, Germany).

Immunofluorescence analysis. Huh7 cells were seeded onto glass coverslips in 24-well plates at a density of 6×10^4 cells per well and infected the next day with DV or DV^{S34L} at a multiplicity of infection (MOI) of 1. Four h postinfection (p.i.), ST-148 was added at a final concentration of 10 μM. For quantification of lipid droplets (LDs) and costaining of capsid with dsRNA, 48 h after infection cells were fixed with 4% paraformaldehyde (PFA) (Applichem GmbH, Darmstadt, Germany), 4% sucrose and processed exactly as previously described by using a rabbit anti-capsid antibody (1:1,000), a mouse anti-dsRNA (1:500), and Bodipy-488 (1:500), which stains neutral lipids (15). Secondary staining was carried out using anti-mouse Alexa 546- and anti-rabbit Alexa-633-conjugated antibodies. All images were processed using the ImageJ software package (National Institutes of Health, Bethesda, MD). The background level, calculated from mock-infected cells, was subtracted (−25 pixel), and the 566- and 488-nm channels were smoothed with the mean function set at 1.0. For visualization and quantification of nuclear and cytosolic capsid, cells were fixed with 4% paraformaldehyde (PFA) for 10 min at room temperature and permeabilized with 0.5% (vol/vol) Triton X-100 in PBS. Primary staining was carried out by 45-min incubation with a mouse

anti-capsid antibody diluted in PBS containing 3% goat serum. After extensive washes with PBS, secondary staining was carried out by a 45-min incubation with an Alexa 568-conjugated secondary antibody diluted 1:1,000 in PBS containing 3% goat serum. Nuclear DNA was stained with 4′,6-diamidino-2-phenylindole (DAPI) (Molecular Probes, Karlsruhe, Germany). For staining of LDs, Bodipy-488 was added (1:500 dilution) to each coverslip for 10 min at room temperature. Samples were mounted on glass slides with Fluoromount G (Southern Biotechnology Associates, Birmingham, AL), and images were acquired using a Leica CTR MIC fluorescence microscope or a Nikon Eclipse Ti spinning-disc confocal laser microscope. Immunofluorescence signals were quantified using ImageJ, and images were assembled with the Adobe Photoshop software package. For quantification of LD size and number, cells were stained as described above and imaged using a 63× objective, and the size and number of Bodipy-488-stained LDs was calculated by using ImageJ. For each condition, at least 10,000 LDs in more than 500 cells and 8 to 10 fields of view were examined.

Infectivity assay. For the determination of virus titers, Huh7 target cells were seeded into 96-well plates (10^4 cells/well) the day before infection. Cells were inoculated with serial dilutions of virus-containing supernatants that had been filtered through a 0.45-μm-pore-size filter. Infected cells were detected by immune staining of the E protein using the mouse anti-E antibody (3H5-1; diluted 1:500) and secondary horseradish peroxidase-conjugated antibody (1:200). Virus titers (the 50% tissue culture infective dose [$TCID_{50}$]/ml) were calculated as previously reported (16).

Determination of antiviral activity of ST-148. Huh7 cells were seeded into 12-well plates at a density of 1×10^5 cells per well and incubated overnight. Cells then were infected with DV, DV^{S34L}, DVR2A, or $DVR2A^{S34L}$ at an MOI of 0.1 in the presence of a range of compound concentrations. Seven compound concentrations (25, 8, 2.5, 0.8, 0.25, 0.025, and 0.008 μM) were used to determine the 50% effective concentration (EC_{50}). After 1 h, inocula were removed and fresh medium containing various concentrations of ST-148 was added to each well. After a 48-h incubation period, supernatants were harvested and filtered through a 0.45-μm-pore-size filter, and 10-fold dilutions were used to determine virus titer by plaque assay as described previously (13). EC_{50}s were calculated by fitting the data to a four-parameter logistic model (variable-slope, nonlinear regression model) to generate a dose-response curve by using the GraphPad Prism 5.0 software package (GraphPad Software, San Diego, CA). From this curve, the concentration of compound that reduced virus-induced cytopathic effect (CPE) by 50% was calculated.

***In vitro* transcription and RNA transfection.** *In vitro* transcripts were generated as previously described (17). For RNA transfection, Huh7 or 293T single-cell suspensions were prepared by trypsinization, washed with PBS, and resuspended at a concentration of 1×10^7 cells (Huh7) or 1.5×10^7 cells (293T) per ml in Cytomix, supplemented with 2 mM ATP and 5 mM glutathione. Ten μg of subgenomic or genomic *in vitro* transcript then was mixed with 400 μl of the cell suspension and transfected by electroporation using a Gene Pulser system (Bio-Rad) and a cuvette with a gap width of 0.4 cm (Bio-Rad) at 975 μF and 270 V. Cells were immediately diluted into 20 ml of DMEM complete and seeded in the appropriate format (1 ml/well in 24-well plates, 2 ml/well in 12-well plates, and 15 ml/dish in 15-cm-diameter dishes).

Lentivirus production. The pWPI-BLR capsid constructs, encoding either the capsid WT or containing the S34L mutation, and the pWPI-Puro-prM-E constructs were cotransfected into 293T cells with plasmids encoding Gag-Pol of HIV and the G protein of vesicular stomatitis virus (ratio, 3:3:1) as previously reported (16). After 48 and 72 h, supernatants were harvested, clarified through 0.45-μm-pore-size filters, pooled, and stored in aliquots at −20°C until use.

Molecular modeling. For protein-protein docking, the NMR structures of DV capsid dimers (PDB entry 1R6R) (12) were used. The 20 dimer models were compared using the MOE Protein Consensus tool (version 2010.10; Chemical Computing Group Inc., Montreal, QC, Canada), and the 5 most different structures were selected for rigid protein-protein docking. Each dimer model was used both with the WT sequence and with the S34L mutation, inserted with the MOE Mutate tool. All structures were prepared using the Schrödinger Maestro protein preparation wizard (version 9.5; Schrödinger, LLC, New York, NY). For each model, protein-protein docking was performed with Schrödinger BioLuminate Piper (version 1.2; Schrödinger, LLC, New York, NY) using the same dimer structure for both receptor and ligand entries. The standard mode was applied, probing 70,000 ligand rotations and giving a 0.21 bonus to the complexes that involved Ser34 in the interactions. The best tetramer model was selected by visual inspection.

All of the molecular dynamics (MD) simulations were computed with GROMACS (version 4.5.3) (18) and the AMBER99 force field. All simulations were performed on both WT and S34L mutant structures; the mutation was inserted starting from the WT structure. Periodic boundary conditions were applied, using a cubic box with 0.9-nm minimum distance between the molecular system and the box. Explicit water molecules described with the TIP3P model were added, and systems were neutralized with the addition of 72 Cl^- ions. Missing ST-2148 topology parameters were computed with Antechamber, which is part of the Amber software package (version AMBER12; University of California, San Francisco, CA). Atom partial charges were obtained with the AM1-BCC charge method, while atom types and force field missing parameters were assigned with the GAFF force field. The coordinate and topology files then were converted into GROMACS-compatible format with the acpype converter (Department of Biochemistry, University of Cambridge, United Kingdom).

Prior to the production simulation, two energy minimizations were performed: first with the steepest descendant and second with conjugate gradient methods. Both energy minimizations were implemented for 3,000 steps (with a step size of 1 fs), with a force tolerance of 100 kJ mol^{-1} nm^{-1} for the steepest descent and of 10 kJ mol^{-1} nm^{-1} for the conjugated gradient. Successively, the protein atoms were constrained with a position restraint of 1,000 kJ mol^{-1} nm^{-2}, and water molecules were relaxed with two 50-ps (50,000 steps, step size of 1 fs) position-restraint MDs. Coordinates, velocities, and energy values were saved every 500 steps in both stages. The first position-restraint MD was conducted under NVT conditions (constant number of atoms, N, volume, V, and temperature, T), allowing the system to be heated to 300 K with v-rescale temperature coupling and 0.1-ps time constant. The second stage then was performed under NPT conditions (with constant number of atoms, N, pressure, P, and temperature, T). Both temperature (with v-rescale, temperature of 300 K and time constant of 0.1 ps) and pressure coupling (with Berendsen algorithm, 1 bar pressure and time constant of 0.5 ps) were applied in this case. A 30-ns (15,000,000 steps with 2-fs step size) production simulation was run for each molecular system under the NPT conditions described above. Coordinates, velocities, and energy values were saved every 1,000 steps. In all procedures, a 0.9-nm short-range cutoff was applied for long-range electrostatic interactions that were calculated with the particle mesh Ewald (PME) method, while short-range nonbonded interactions were calculated within a cutoff of 1.4 nm.

For ST-148 docking, each small-molecule docking simulation was performed using Schrödinger Maestro (version 9.5; Schrödinger, LLC, New York, NY). Prior to docking, the protein and ST-148 were prepared with the protein preparation wizard tool and LigPrep, respectively, generating all possible tautomers and ionization states at pH 7.0 ± 2.0. For each docking, the grid was generated with Glide, defining appropriate center and box sizes. Docking was performed with Glide standard precision (SP) mode, sampling nitrogen inversions and ring conformations and penalizing nonplanar conformations for amides. The 25 poses generated then were refined with the SP mode.

Plasmid constructs. Plasmids carrying the subgenomic replicon (pFK-sgDVsR2A) and the full-length genomes, pFK-DVs and pFK-DVs.R2A (carrying a *Renilla* luciferase reporter gene), are based on the DV-2 16681 strain and have been described recently (17) (Fig. 1A). The S34L amino acid substitution conferring resistance to ST-148 was intro-

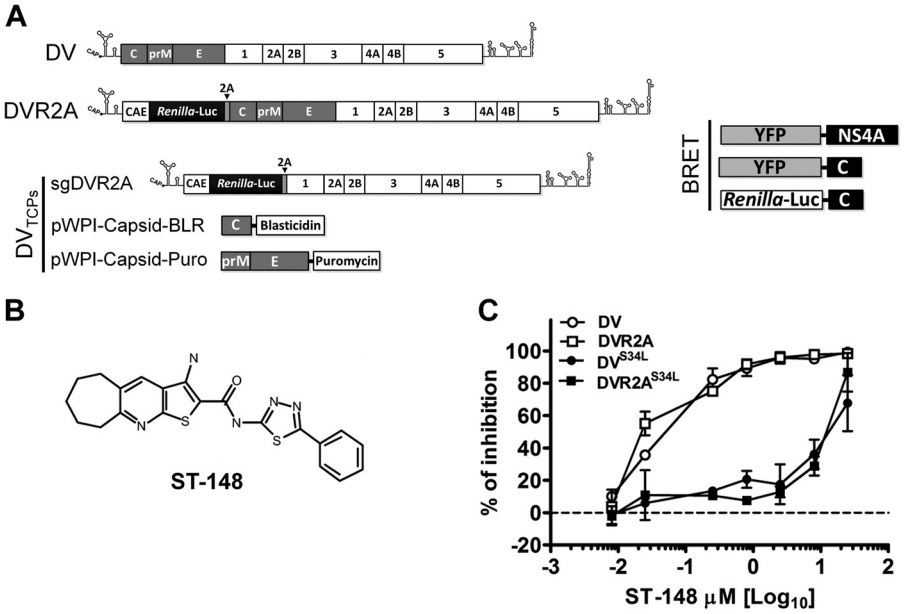

FIG 1 Schematic representation of constructs used in this study and antiviral potency of ST-148. (A) Schematic representation of genomic and subgenomic constructs. The DV2 full-length genome is shown at the top (DV). The 5′ and 3′ N terminal regions are depicted with their putative secondary structures. Polyprotein cleavage products are separated by vertical lines and labeled as specified in the introduction. DVR2A is derived from the DV2 full-length genome by insertion of a *Renilla* luciferase coding sequence preceded by the capsid cyclization sequence (CAE) and followed by a *Tosea asigna* virus 2A cleavage site. The middle panel depicts the constructs used for production of *trans*-complemented DV particles (DV_{TCP}). sgDVR2A is a subgenomic reporter replicon that is packaged into virus-like particles by the capsid and prM/envelope proteins transiently expressed in *trans* via two different lentiviruses (pWPI capsid-BLR and pWPI prME-Puro, respectively). All constructs are derived from the DVs2 16681 isolate (17). The right panel depicts the constructs used for BRET experiments. YFP and *Renilla* luciferase proteins were N-terminally fused to either capsid or NS4A of DV2 (strain 16681). (B) Structure of ST-148. (C) Antiviral potency of ST-148. Huh7 cells were infected at a DV or DVR2A reporter virus MOI of 0.1, with the virus containing or not containing the resistance mutation S34L, for 60 min at 37°C in the presence of various concentrations of the compound. After removal of the inoculum and several washings with PBS, cells were incubated with fresh medium containing various concentrations of ST-148 or DMSO. After 48 h, virus amounts released into the supernatant were determined by PFU assay with VeroE6 cells. Data represent averages and error ranges from two independent experiments.

duced into the capsid coding region by site-directed mutagenesis using PCR with the external primers capsid_AgeI_frw (5′-AACAAACCGGTA GAGCCGAGGGCAG-3′) and capsid_NaeI_rev (5′-TAATGATCATGC CGGCAGATCTGCG-3′) and the internal primers capsid_S34L_frw (5′-CAAAGAGATTCCTACTTGGAATGCT-3′) and capsid_S34L_rev (5′-A GCATTCCAAGTAGGAATCTCTTTG-3′; mutated codons are underlined) and inserted into pFK_DVs and pFK_DVsR2A via AgeI/NaeI restriction sites. Numbers given refer to amino acid positions in the capsid open reading frame. For BRET experiments, Gateway technology was employed. The WT or S34L capsid coding regions as well as the DV NS4A coding region (which served as a negative control) were amplified by PCR using full-length genomes as the templates and the external primers s_mC_LM_N (5′-TAGGTACCGGATGAATAACCAACGGAAAAAGG-3′), as_mC_LM_N (5′-TAGATATCCTATCTGCGTCTCCTATTCAAG ATG-3′), s_NS4A_LM_N (5′-TAGGTACCGGTCTCTGACCCTGAAC CTAATCACAG-3′), and as_NS4A_LM_N (5′-TAGATATCCTATCTCT GTTTTTCAGGTTCTGG-3′) to generate intermediate entry clones. Amplicons were inserted into the entry vector backbone (pENTR4 vector; Invitrogen, Karlsruhe, Germany) via KpnI/EcoRV restriction sites. Gateway destination clones encoding humanized *Renilla* luciferase and YFP were generated using standard cloning PCR-based procedures, creating pT-Rex-DEST30-nt-RL and pT-RexTM-DEST30-nt-YFP plasmids. Finally, expression clones were generated by LR reaction according to the manufacturer's instructions, with slight modifications. Briefly, 150 ng entry clone, 150 ng destination vector, 1 μl LR clonase enzyme mix, adjusted to a total volume of 10 μl with 10 mM Tris-HCl (pH 8.0), was incubated at 25°C for 2 h or overnight. The reaction was stopped by the addition of 1 μl Proteinase K (2 μg/μl) and incubation at 37°C for 10 min. Finally, the complete reaction mixture was transformed into competent *Escherichia coli* DH5α cells. Isolated plasmids were sequence verified, and expression was confirmed by Western blot analyses of transfected cells and by fluorescence microscopy (data not shown). For the production of lentiviruses expressing the structural proteins, the capsid and prM-Envelope coding sequences were amplified by PCR using full-length genomes as the template and the following primers containing the given unique restriction sites, an AUG initiation codon, and a stop codon at the 3′ end: capsid_SbfI_frw (5′-ATGTATGTCCTGCAGGGCCACCATGAATAACCAACG GAAAAAGGCGAAAAAC-3′), capsid_MluI_rev (5′-CTAACATTTAC GCGTCTATCTGCGTCTCCTATTCAAGATGTTCA-3′), prM-E_SbfI_ frw (5′-TATGTCCTGCAGGGCCACCATGAGAGCCGAGGGCA-GGG GAAGTCTTCTAACATGCGGGGACGTGGAGGAAAATCCCGGGCC CTCTGCCGGCATGATCATT-3′), and Env_MluI_rev (5′-CTAACA TTTACGCGTCTAGGCCTGCA-CCATGACTCCCAAATACAGT GT-3′). A *Thosea asigna virus* (TaV) 2A coding sequence, mediating self-cleavage, was inserted upstream of the capsid anchor sequence to ensure cleavage at the capsid-anchor junction. The capsid coding region was inserted into a pWPI-BLR vector carrying the blasticidin resistance gene, and the prM-E cassette was inserted into a pWPI-Puro vector encoding a puromycin resistance gene as previously described (16). All constructs were verified by nucleotide sequence analysis.

qRT-PCR analysis. Total cellular RNA from ~5×10^5 virus-infected cells and 1/10 of the corresponding supernatants was isolated by using the NucleoSpin RNA II kit (Macherey-Nagel, Düren, Germany) as recommended by the manufacturer. The cDNA was prepared using a high-capacity cDNA reverse transcription kit (Applied Biosystems, Life Technologies). Quantitative real-time PCR (qRT-PCR) was carried out using an ABI Prism 7000 sequence detector system (Applied Biosystems, Foster City, CA). For each primer set, reactions were conducted in triplicate by

using the Green Dye RT-PCR master mix (PJK GmbH, Hilden, Germany) according to the manufacturer's instructions, with the following primers binding to a region within the DV NS5 coding sequence (primer polarities are indicated): sDV2-9687 (5′-GCCCTTCTGTTCACACCATT-3′; forward) and asDV2-9855 (5′-CCACATTTGGGCGTAAGACT-3′; reverse). The total volume of the reaction mixture was 15 μl, and reactions were performed in two stages: stage 1, 15 min at 95°C; stage 2, 40 cycles of 15 s at 95°C and 60 s at 60°C. Quantities of DV RNA were calculated by using serial dilutions of known amounts of DV *in vitro* transcripts that were processed in parallel as previously described (19).

Sequence alignments. Sequence alignments were performed with the following flaviviruses (UniprotKB/Swiss-Prot accession numbers are given): DV-1 (Brazil/97-11/1997), P27909; DV-2 (Thailand/16681-PDK53), P29991; DV-3 (Martinique/1243/1999), Q6YMS3; DV-4 (Thailand/0348/1991), Q2YHF0; West Nile virus, P06935; yellow fever virus (Ivory Coast/1999), Q6J3P1; Japanese encephalitis virus (SA-14), P27395; Kunjin virus (MRM61C), P14335; and St. Louis encephalitis virus (MS1-7), P09732.

Statistical analyses. Statistical analyses were performed by applying the two-tailed, unpaired Student's *t* test. In some cases, indicated in Results, data were analyzed with one-way analysis of variance (ANOVA) and Dunnett's *post hoc* test for multiple comparisons to nontreated controls or ANOVA and Tukey's *post hoc* test to compare every group to each other, as indicated in the figure legends. Microsoft Excel and GraphPad Prism (v. 5.0) were used for statistical analyses.

Subcellular fractionation. For subcellular fractionation of cytosolic, membrane, nuclear, and postnuclear fractions, the Qproteome cell compartment kit, purchased from Qiagen (Hilden, Germany), was used as recommended by the manufacturer. In brief, 10^6 Huh7 cells were seeded into 10-cm-diameter dishes the day before infection. Cells were infected with either DV WT or DV^{S34L} at an MOI of 1 for 4 h at 37°C and washed three times with PBS, and then complete medium containing 10 μM ST-148 or DMSO was added to the cells. After 48 h, cells were washed 3 times with ice-cold PBS, trypsinized, and collected by 5 min of low-speed centrifugation (700 × *g*). Collected fractions were acetone precipitated overnight at −20°C and resuspended in equal volumes of 2× SDS loading buffer. One-tenth of the total cell suspension was saved as the input, and equal amounts of each fraction were subjected to SDS–12% PAGE as described above. Fraction purity was evaluated by determining amounts of cytosolic (GAPDH), membrane (ATP5B), nuclear (lamin A/C), and postnuclear/cytoskeletal (vimentin) markers.

Production of *trans*-complemented DV particles. To produce *trans*-complemented DV particle (DV_{TCP}) stocks, 293T cells were electroporated with 10 μg of subgenomic DVR2A (sgDVR2A) replicon RNA, seeded into 15-cm-diameter dishes, and incubated at 37°C. The next day, cells were inoculated with lentiviral particles encoding capsid and prM-E for 8 h. Cells were washed carefully 3 times with PBS, fresh medium was added, and cells were cultured at 33°C for 4 to 6 days. Supernatants were pooled and filtered through a 0.45-μm-pore-size filter, and 15 mM HEPES (pH 7.2 to 7.5) was added to the medium. DV_{TCP} stocks were stored in aliquots at −80°C until use.

Transient replication assay and DV_{TCP}-based virus entry assay. Huh7 cells transfected with full-length DVR2A RNA were seeded into 12-well plates. Replication was determined by measuring luciferase activity in cell lysates 4, 24, 48, and 72 h after transfection. For harvest, cells were washed once with PBS and lysed by adding 200 μl lysis buffer as previously described (19). Cells were frozen immediately at −70°C, and after thawing, lysates were resuspended by gentle pipetting. For each well, 20 μl lysate, mixed with 400 μl assay buffer (25 mM glycylglycine, 15 mM $MgSO_4$, 4 mM EGTA, 1 mM DTT, 2 mM ATP, 15 mM K_2PO_4 [pH 7.8], 1.42 μM coelenterazine H), was measured for 10 s in a luminometer (Lumat LB9507; Berthold, Freiburg, Germany). Each well was measured in duplicate. To determine the amount of infectious virus particles released into culture supernatants 72 h after electroporation, naive Huh7 cells were inoculated with these supernatants, and 48 h later luciferase activity was determined. Kinetics of virus replication were calculated by normalizing the relative light units (RLU) measured at a given time point to the respective 4-h value. Four-hour values, reflecting transfection efficiency, were comparable among samples and biological replicates, and no statistically significant differences were observed. For DV_{TCP} experiments, Huh7 cells were inoculated with particles composed of WT capsid protein or containing the S34L resistance mutation for 90 min at 37°C. At different times before, during, or after inoculation, 10 μM ST-148 or 0.1% DMSO was added to the medium. Replication was measured 48 h after inoculation.

Virucidal assay. Preparations of DV and DV^{S34L} particles (corresponding to 3.8×10^6 $TCID_{50}$/ml) were incubated for 1 h at 37°C in DMEM containing 10 μM ST-148 or 0.1% DMSO. Viruses were serially diluted, and the remaining infectivity was measured by $TCID_{50}$ assay.

Analysis of infected cells by transmission electron microscopy. Huh7 cells (6×10^4) were seeded onto glass coverslips, and around 16 h later, cells were infected with either DV or DV^{S34L} at an MOI of 3. After 4 h, cells were washed three times with prewarmed PBS, and DMEM containing 10 μM ST-148 or 0.05% DMSO was added. After a 48-h incubation period, cells were fixed and prepared for transmission electron microscopy as described previously (20).

TABLE 1 Antiviral activity of ST-148 against DV 16681-based viruses

Virus	EC_{50}[a] (μM)
DV2	0.052 ± 0.016
DVR2A	0.037 ± 0.028
DV^{S34L}	11.79 ± 2.34
$DVR2A^{S34L}$	11.14 ± 3.27

[a] Cells were infected with given viruses at an MOI of 0.1 and treated with ST-148. Culture medium was collected 48 h postinfection, and virus titers were determined by plaque assay (Huh7 cells; $CC_{50} > 100$ μM as determined in reference 13). Data represent averages and error ranges from two independent experiments.

RESULTS

ST-148 is a potent inhibitor of DV. ST-148 (Fig. 1B) was identified by a high-throughput screen as a potent inhibitor of DV, exhibiting antiviral activity against all four serotypes and reducing viremia *in vivo* (13). In the first set of experiments, we confirmed the antiviral potency of ST-148 by using synthetic DV-2-based clones derived from the isolate 16681 (Fig. 1A) (17), which was used throughout the study. To determine the inhibitory potency of the compound, Huh7 cells were infected with DV or the DVR2A luciferase reporter virus, encoding either the WT or the previously identified ST-148 resistance mutation in capsid protein (S34L). Released infectivity was assessed by a PFU titration assay using culture supernatants harvested 48 h after infection. As previously observed for the DV-2 NGC strain (13), ST-148 also inhibited 16681-derived DV with EC_{50}s in the low-nanomolar range (52 and 37 nM, respectively) (Fig. 1C and Table 1). These values were around 220- to 300-fold higher in the case of the DV^{S34L}- and $DVR2A^{S34L}$-resistant mutants, respectively, corroborating our previous findings and validating the antiviral potency of ST-148 independent of the DV strain used.

ST-148 does not affect viral RNA replication but inhibits DV spread. Previous time-of-addition studies have shown that ST-148 is effective when added up to 12 h postinfection, suggesting a postentry mechanism of action (13). However, the virus yield inhibition assays used allowed several cycles of viral replication; therefore, possible effects on DV entry, viral RNA replication, and assembly or release of virus particles could not be distinguished. In order to dissect the possible impact of ST-148 on different steps of the viral replication cycle, we first assessed viral RNA replication

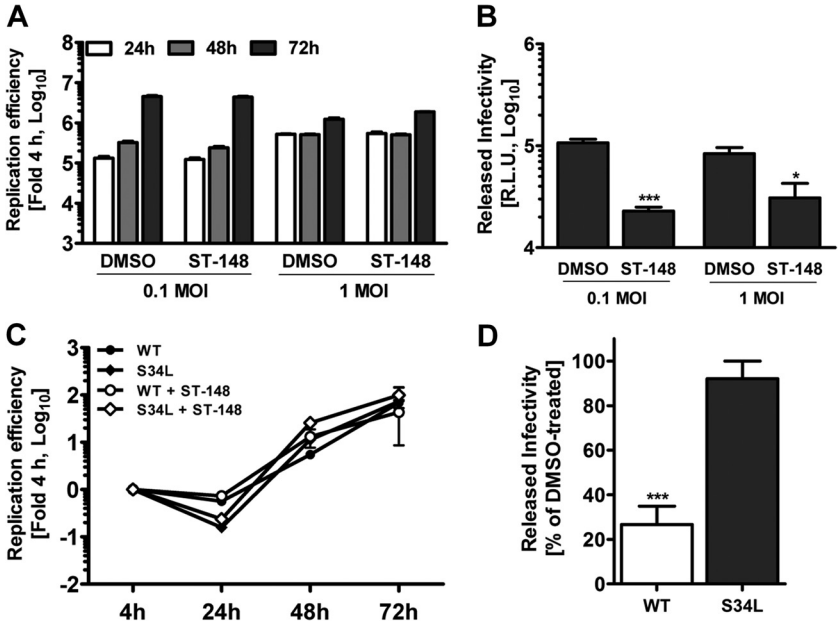

FIG 2 ST-148 does not affect viral RNA replication but reduces production of infectious DV particles. (A) No effect of ST-148 on replication kinetics of the DVR2A reporter virus. Huh7 cells were infected with DVR2A at an MOI of 0.1 or 1 for 4 h at 37°C, washed with PBS, and incubated with fresh medium containing 5 μM ST-148 or DMSO. At the indicated time points after infection, luciferase activity was measured in the lysates as described in Materials and Methods. Note that error bars are poorly visible due to the size of the graph. (B) Reduction of virus production by ST-148. Supernatants of infected cells treated with 5 μM ST-148 were harvested 72 h postinfection and used to infect naive Huh7 cells. After 48 h, cells were harvested and luciferase activity was determined. (C) Comparison of replication kinetics of DVR2A and DVR2A^{S34L} in the presence or absence of ST-148. Huh7 cells were electroporated with 10 μg of capped *in vitro* transcripts of WT DVR2A or DVR2A^{S34L} (S34L), and 4 h later, 5 μM ST-148 or DMSO was added to the medium. At time points specified at the bottom, luciferase activity was determined. (D) Inhibition of virus production by DVR2A- and DVR2A^{S34L}-transfected cells upon ST-148 treatment. Supernatants of transfected and ST-148-treated cells were harvested 72 h postinfection and used to infect naive Huh7 cells. After 48 h, cells were harvested and luciferase activity was determined. Data shown in each panel represent averages and standard deviations from three independent experiments (***, $P < 0.001$; *, $P < 0.05$).

and virus spread by using a DVR2A luciferase reporter virus and addition of ST-148 4 h postinfection, i.e., after virus entry had taken place. Virus replication in infected cells was determined 24, 48, and 72 h after infection by luciferase assay (Fig. 2A). Effects on virus production were quantified by using culture supernatants of infected and drug-treated cells harvested 72 h after inoculation, infection of naive Huh7 cells, and measuring luciferase activity 48 h later (Fig. 2B). While viral RNA replication was not affected by ST-148, luciferase counts detectable in the reinfection assay were decreased 60 to 80%, arguing that the compound reduced virus production (Fig. 2A and B, respectively).

To corroborate that the antiviral effect of ST-148 observed was due to virus production and independent from virus entry under these conditions and to investigate the phenotype of the ST-148-resistant mutant, we next determined the replication competence of either virus in Huh7 cells that had been transfected with the corresponding DV genomes, deliberately bypassing the entry step. Under these conditions, both viruses replicated comparably regardless of ST-148 treatment (Fig. 2C). However, a significant ~80% reduction of amounts of infectious virus was observed exclusively for the WT virus (Fig. 2D), confirming a selective inhibition of the late steps of the DV replication cycle by ST-148.

ST-148 inhibits the production of infectious DV particles. In order to determine whether the reduction of virus production resulted from an impairment in virus particle release or a reduction of their specific infectivity, we next performed infectivity and viral RNA titration experiments. Huh7 cells were infected with 1 MOI of DV, and various concentrations of ST-148 were added 4 h after infection. Amounts of released viral RNA and infectious DV particles in the supernatant were determined 48 h later by qRT-PCR and $TCID_{50}$ assay, respectively (Fig. 3A and B). These experiments revealed a dose-dependent reduction of virus titers as deduced from the up to 10-fold smaller amounts of infectivity and viral RNA observed at the highest inhibitor concentration.

We next investigated whether the observed reduction of virus titer resulted from an impairment of virus spread or from a direct block in virus particle production by using a single-cycle infection experiment. Huh7 cells were infected with DV or DV^{S34L} at an MOI of 1 and incubated for 48 h to allow for nearly complete infection of the cell monolayer (Fig. 3C). Released viruses then were removed by extensive washing, and medium containing DMSO, ST-148, or brefeldin A, which served as a positive control, was added to the cells. Cells were incubated for just 12 h, which is the estimated length of a single complete DV replication cycle (21 and B. Schmid, unpublished observations). Therefore, reinfecting or superinfecting virus produced within this time period would not significantly contribute to extracellular virus titer. Viral RNA contained within infected cells or released into the culture supernatant was quantified by RT-qPCR. In addition, infectivity titers were determined by limiting-dilution assay. Under these conditions, a highly significant reduction of ~90% of infectivity was observed for the drug-treated WT virus, while the S34L mutant was unaffected by ST-148 treatment (Fig. 3D). Concomitantly, ST-148 profoundly reduced secretion of viral RNA by ~70% in the case of DV WT, while no statistically significant reduction could be observed for the DV^{S34L}-resistant variant (Fig. 3E). As

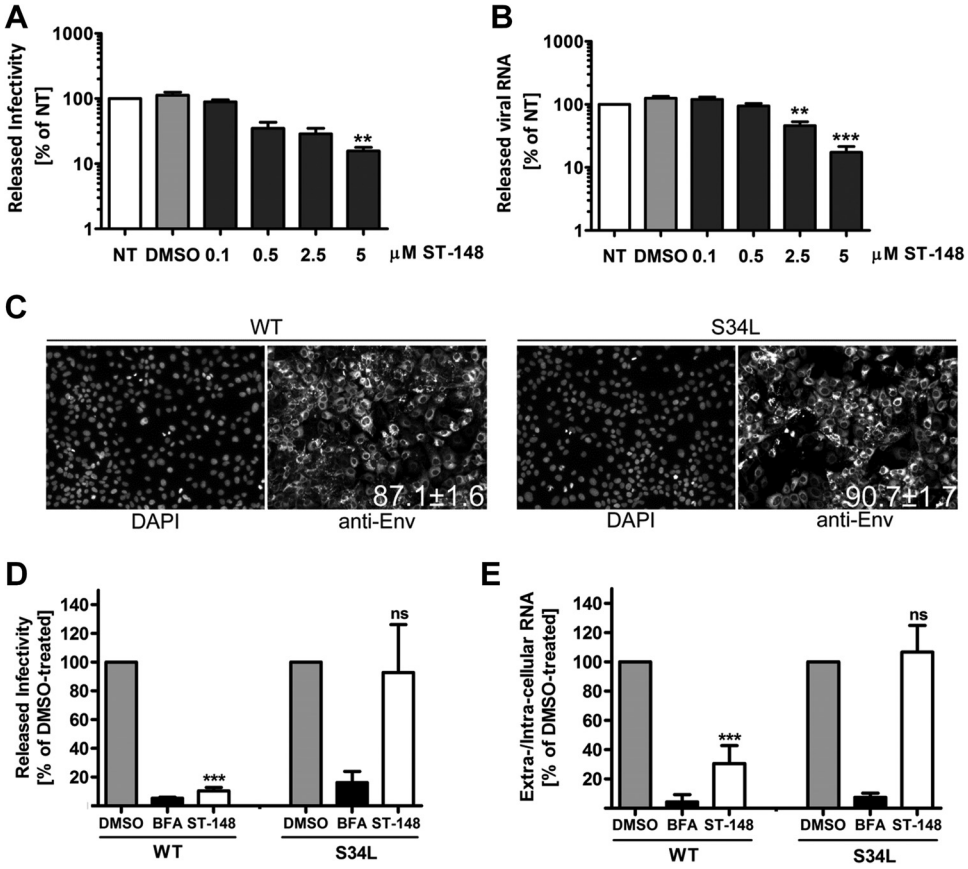

FIG 3 Inhibition of the release of infectious DV particles by ST-148 as revealed by single-cycle experiments. (A) Production of infectious extracellular DV upon ST-148 treatment. (B) Quantification of released viral RNA. Huh7 cells were infected with DVR2A at an MOI of 1 for 4 h at 37°C, washed with PBS, and incubated with fresh medium (nontreated [NT]) or medium containing DMSO or the given concentrations of ST-148. After 48 h, clarified supernatants were used for $TCID_{50}$ assay to quantify infectivity titers or two-step qRT-PCR for quantification of viral RNA amounts released into the supernatant. Data were analyzed using one-way ANOVA and Dunnett's *post hoc* test (**, $P < 0.01$; ***, $P < 0.001$). (C) Determination of infection efficiency. Cells were infected with DV or DV^{S34L} and 48 h later were fixed and analyzed by immunofluorescence using a DV E-specific antibody. Nuclear DNA was stained with DAPI. Numbers in the lower right of the panels refer to the percentage of infected cells (means from at least 1,500 cells ± standard deviations). (D and E) Effect of ST-148 on single-round DV particle release. Huh7 cells were infected with DV or DV^{S34L} for 48 h, washed extensively with PBS, and incubated for 12 h with medium containing 0.1% DMSO, 1 μg/ml brefeldin A (BFA), or 10 μM ST-148. Released infectivity and viral RNA were quantified by $TCID_{50}$ assay and qRT-PCR, respectively. Results represent means and standard deviations from at least 3 independent experiments. (ns, nonsignificant; *, $P < 0.05$; ***, $P < 0.001$).

expected, in both cases BFA treatment drastically reduced titers of both viral RNA and infectivity (Fig. 3D and E; black columns), consistent with an earlier report (22). In conclusion, these results suggest that ST-148 reduces DV particle production. The concomitant reduction of extracellular infectivity and viral RNA amounts implies that ST-148 has no significant effect on specific infectivity of DV particles.

ST-148 additionally inhibits DV entry. Since viral RNA replication in the presence of ST-148 was unaltered and the observed inhibitory effect of the drug on assembly/release of DV particles was rather modest compared to the high inhibitory potency observed by virus yield inhibition assay, we hypothesized that ST-148 has an additional effect on virus entry. To verify this hypothesis, we developed a *trans*-complementation system, which allows production of infectious virus-like particles containing a subgenomic replicon that are unable to spread in cell culture (23, 24, 25, 26, 27). These particles, which we call DV *trans*-complemented particles (DV_{TCP}), in analogy to our earlier report on HCV_{TCP} (16), were obtained by transfecting subgenomic replicons into helper cells that provide the structural proteins in *trans* (Fig. 4A). Since packaged subgenomic replicon RNAs lack the region encoding the structural proteins, DV_{TCP} only support a single round of infection. Moreover, DV_{TCP} encode the *Renilla* luciferase reporter gene; therefore, single-round infection can be measured as a function of luciferase activity.

Taking advantage of luciferase-encoding DV_{TCP} composed of WT or S34L capsids, we performed time-of-addition studies by treating cells before, during, or at different times after infection with ST-148 and measured luciferase activity 48 h later. As shown in Fig. 4B, maximal antiviral activity was achieved when cells were treated prior to or during infection, reducing viral replication up to 70% ($P < 0.001$). Significant antiviral effect was still obtained up to 120 min postinfection (i.e., 30 min after removal of virus inoculum), whereas treatment at later time points had no effect (Fig. 4B).

To exclude a general nonspecific virucidal effect of ST-148 on DV particles, we incubated high-titer virus stocks of DV or DV^{S34L} with 10 μM ST-148 for 1 h at 37°C and determined the infectivity titer after extensive dilution by $TCID_{50}$ assay (Fig. 4C). Under these conditions, no significant reduction of viral infectivity could be observed. Taken together, these data sug-

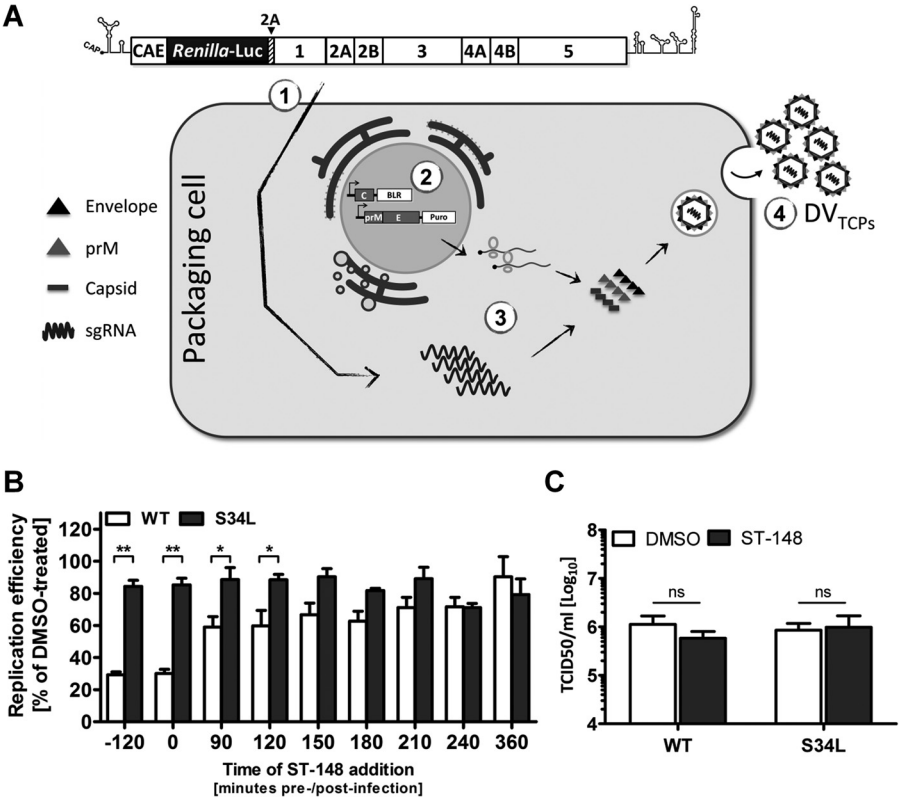

FIG 4 ST-148 additionally inhibits DV particle entry. (A) Schematic representation of the system used to produce *trans*-complemented DV particles (DV_{TCP}). 293T cells were electroporated with 10 μg of capped *in vitro* transcripts of the subgenomic replicon sgDVR2A (segment 1). The next day, cells were transiently transduced with lentiviruses expressing the structural proteins capsid (wild type or containing the ST-148 resistance mutation S34L) and prM-E (segment 2). Replicating viral RNA is packaged in *trans* (segment 3), giving rise to DV_{TCP} stocks that are released into the culture supernatant and harvested 4 to 6 days after transduction (segment 4). (B) Effect of ST-148 on entry of DV_{TCP}. Huh7 cells were infected with DV_{TCP} (WT or the S34L mutant) for 90 min at 37°C. The inoculum was removed and fresh medium was added. At time points specified at the bottom of the graph, medium was replaced by medium containing 10 μM ST-148 or 0.1% DMSO. In one case (−120 min), cells were pretreated with ST-148 for 2 h prior to infection. Cells were harvested 48 h postinfection, and luciferase activities in the lysates were measured. (C) No virucidal effect of ST-148. Stocks of DV WT or DV^{S34L} were incubated at 37°C for 1 h with 10 μM ST-148 or 0.1% DMSO and used to determine infectivity titers by limiting-dilution assay ($TCID_{50}$). Data represent averages and standard deviations from three independent experiments (ns, nonsignificant; *, $P < 0.05$; **, $P < 0.001$).

gested that ST-148 specifically blocks DV entry, which is not due to a virucidal effect.

ST-148 does not affect colocalization of capsid with lipid droplets and dsRNA but increases clustering of virus particles in the ER. In DV-infected cells, C protein resides both in the cytoplasm and nucleus (28, 29, 30). Cytosolic capsid protein was shown to localize around LDs (15) and in close association with vesicle packets, which are sites of RNA replication (30, 31, 32), while nuclear capsid protein accumulates in nucleoli and was reported to interact with nuclear proteins (33, 34, 35). In order to investigate whether ST-148 would affect the recruitment of capsid to LDs and its colocalization with dsRNA, we performed colocalization studies using DV-infected cells treated with ST-148. Treatment was started 4 h postinfection until cells were fixed by using paraformaldehyde and a low concentration of Triton X-100 as reported earlier (15). As shown in Fig. 5A, we could not observe a difference between inhibitor- and DMSO-treated cells, and colocalization of capsid around LDs or with dsRNA appeared unaltered. To rule out possible effects of ST-148 on LD morphology or abundance, we quantified their average sizes and numbers per cell (Fig. 5B and C). While LD size was comparable between DMSO- and ST-148-treated cells, the overall amount of LDs per cell appeared slightly reduced upon drug treatment; however, this difference was not statistically significant. In agreement with previous reports (15), we observed an increase in the overall amount of LDs/cell in DV infected cells (Fig. 5C). These results indicate that ST-148 does not alter recruitment of capsid around LDs or its colocalization with dsRNA.

With the aim of gaining insights into the mode of action of ST-148, we next investigated the effect of the compound on the ultrastructural morphology of DV-infected cells treated with ST-148 by using transmission electron microscopy (Fig. 5D). Both DV- and DV^{S34L}-infected cells contained the characteristic membrane invaginations, which have been proposed to represent viral replication factories (vRFs) (9), and virions forming regular arrays within the ER. Treatment of DV-infected cells with ST-148 did not affect the morphology of vRFs, consistent with a lack of inhibition of viral RNA replication, whereas the overall amount of virions was drastically reduced. Interestingly, in the case of the WT virus, the fewer virions that could be found intracellularly in ST-148-treated cells appeared to form larger arrays than control cells (Fig. 5E). This phenotype was specific and not found with ST-148-treated cells that had been infected with the DV^{S34L}-resistant mutant (Fig. 5E).

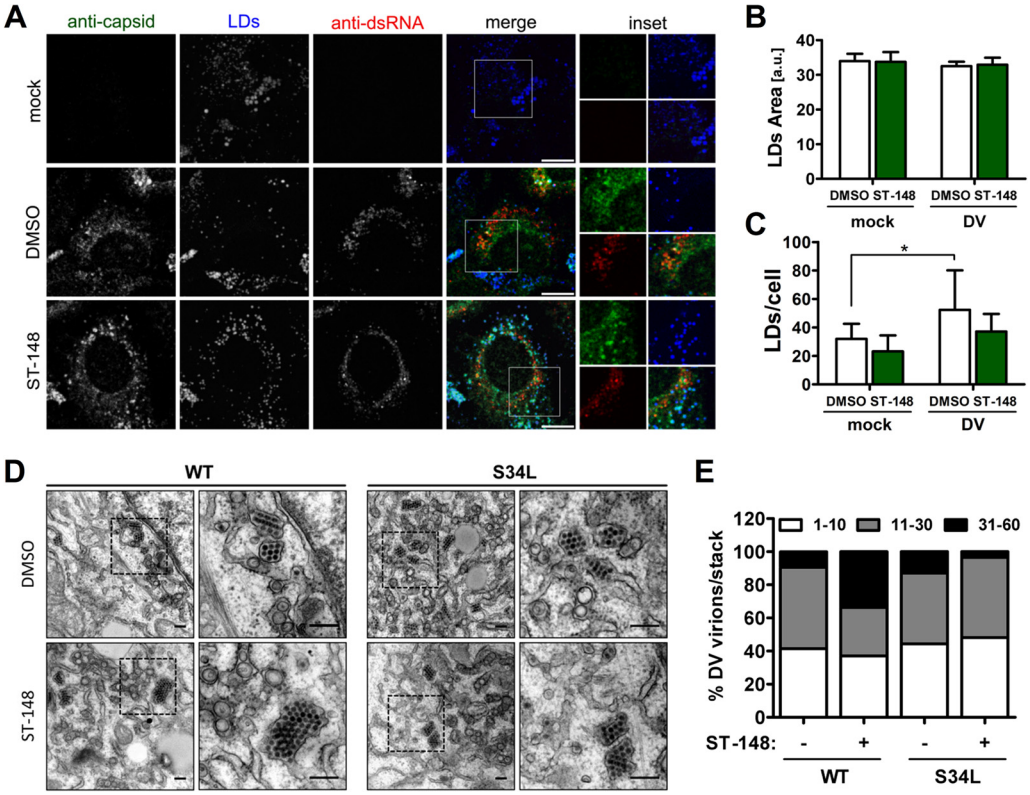

FIG 5 Effect of ST-148 on subcellular localization of viral RNA and protein and accumulation of DV particles in ER stacks. (A) Colocalization of capsid with dsRNA and LDs in ST-148 treated cells. Huh7 cells were infected with DV WT at an MOI of 1, and 4 h later, DMSO or 10 μM ST-148 was added to the medium. After 48 h, cells were fixed with 4% PFA in 4% sucrose. To visualize cytosolic LD-associated capsid protein, cells were permeabilized with 0.1% Triton X-100 and incubated with a rabbit polyclonal anti-capsid antibody, mouse anti-dsRNA antibody, and Bodipy-488 (to detect LDs). Scale bars represent 10 μm. (B and C) Impact of ST-148 on LD size and number, respectively. The mean area and number of LDs per cell has been calculated by using the Fiji plug-in of ImageJ. Each data set represents averages and standard deviations from at least 500 cells per condition (a.u., arbitrary units; *, $P < 0.05$). (D) Accumulation of DV particles in ER stacks upon ST-148 treatment. Huh7 cells were infected with DV WT or the DV^{S34L} mutant (S34L) at an MOI of 3. Four hours after infection, the inoculum was removed and cells were incubated for 44 h in the presence of 10 μM ST-148 or DMSO. Cells were fixed, processed, and analyzed by transmission electron microscopy as described in Materials and Methods. The areas boxed in the left panels are shown at higher magnification on the right. Scale bars in each panel represent 200 nm. (E) Quantification of intracellular DV particle distribution. The number of virions present in ER stacks was quantified and assigned to 3 categories according to the number of virions per stack. Each column represents the mean of at least 1,000 virions from at least 15 infected cells per condition.

ST-148 alters intracellular distribution of capsid protein. Several lines of evidence point toward a functional role for flavivirus capsid within the nucleus of infected cells. For instance, West Nile virus capsid protein has been proposed to dynamically shuttle between the cytoplasm and the nucleus, and the temporal regulation of this process was suggested to prevent premature encapsidation of viral RNA at early stages of infection (33, 36). For Japanese encephalitis virus, it was shown that disrupting nuclear localization affected virus replication and pathogenesis in mice (37). In the case of DV, several studies reported the presence of C protein in the nucleoli of infected cells (28, 33, 34, 38). Moreover, DV C protein has been shown to interact with a number of nuclear proteins, including hnRNP-K and histones (39, 40, 41); however, the relevance of nuclear localization of DV C protein with respect to viral replication is unclear (28). In light of these reports, we investigated the influence of ST-148 on the nuclear accumulation of C protein by using an immunofluorescence protocol that includes the permeabilization of the nucleus. Consistent with earlier reports (15), under these conditions we detected capsid both in the cytosol and within the nucleoli of infected cells (Fig. 6A and B). In the case of DV WT-infected cells, ST-148 treatment increased capsid accumulation within the nucleoli compared to that of DMSO-treated control cells. In contrast, although the S34L-containing capsid protein exhibited enhanced nuclear localization, this subcellular distribution was not affected by ST-148 treatment.

To further investigate the intracellular distribution of C protein upon ST-148 treatment, we generated subcellular fractions of DV- or DV^{S34L}-infected cells by using a method that allows separation of cytosolic, membrane, nuclear, and insoluble postnuclear proteins (Fig. 6C). This approach revealed that ST-148 treatment reduced the abundance of cytosolic WT C protein, concomitant with an increase of this protein in the postnuclear, insoluble fraction (Fig. 6C). In contrast, subcellular distribution of the S34L capsid protein was not affected by the treatment of infected cells with the compound (Fig. 6C). In conclusion, these results show that ST-148 reduces the abundance of cytosolic capsid concomitant with an accumulation of the protein in nuclear, detergent-resistant aggregates, which might contribute to the observed reduction of virus particle production.

ST-148 increases capsid self-interaction. DV capsid forms dimers (10) and, eventually, oligomers during nucleocapsid assembly. It is plausible to assume that the stability of capsid oligom-

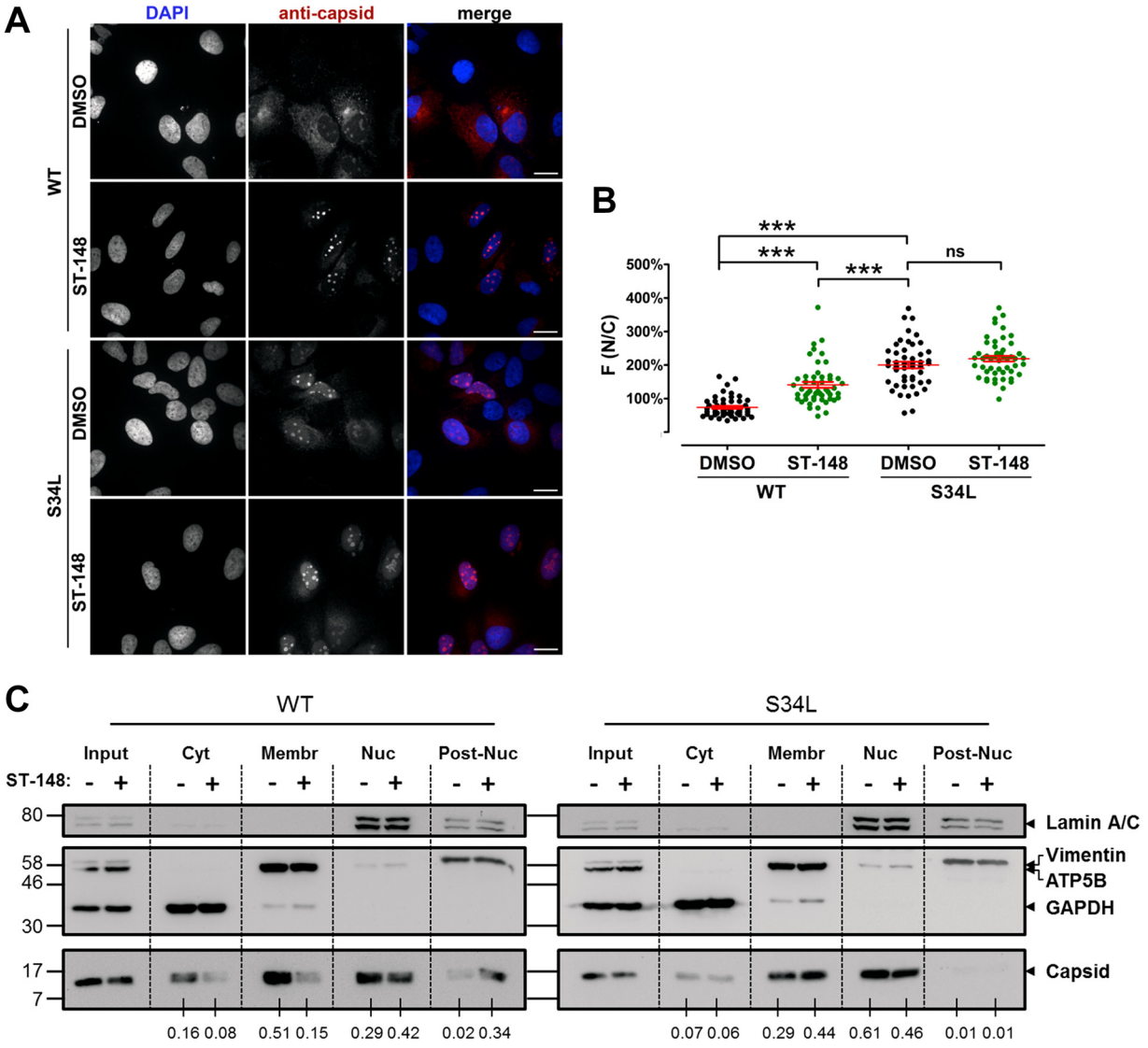

FIG 6 ST-148 induces accumulation of capsid protein in nuclear insoluble aggregates. (A) Intracellular distribution of capsid protein upon ST-148 treatment. Huh7 cells were infected with DV or DV^{S34L} at an MOI of 1, and 4 h later, DMSO or 10 μM ST-148 was added to the medium. After 48 h, cells were fixed with 4% paraformaldehyde, permeabilized with 0.5% Triton X-100, and immune stained for capsid with a mouse monoclonal antibody. Scale bars represent 20 μm. (B) Image-based quantification of intracellular distribution of capsid protein. The extent of nuclear localization of capsid was determined by quantifying capsid-specific signals detected in the nucleus (N) and the cytoplasm (C), respectively, and calculating the ratio of mean fluorescence (*F*) in these two compartments [*F*(N/C)]. Results represent the means ± standard errors of the means ($n \geq 50$). Data were analyzed using one-way ANOVA with Tukey's *post hoc* test (***, $P < 0.001$; ns, nonsignificant). (C) Subcellular fractionation of DV proteins. Huh7 cells were infected with DV or DV^{S34L} at an MOI of 1, and 4 h later, cells were treated with DMSO or 10 μM ST-148. Intracellular distribution of capsid in soluble cytosolic (Cyt), membrane-associated (Membr), nuclear (Nuc), and postnuclear insoluble (Post-Nuc) fractions was evaluated by Western blotting. GAPDH, ATP5B, lamin A/C, and vimentin served as specificity controls for the various fractions. Numbers below each lane refer to the relative amounts of C proteins as determined by densitometry. After subtraction of the background, capsid-specific signals in each fraction were normalized to the corresponding input and expressed as a fold of total signal in the four fractions. Numbers on the left refer to the positions of molecular weight standards (in thousands). One result from two independent experiments is shown.

ers is important for assembly of infectious virus particles and for uncoating during virus entry. Since ST-148 appeared to affect both the efficiency of virus production and entry properties of DV particles, we assumed that this compound affects capsid self-interaction. To address this assumption, we used a BRET-based assay, which allows investigating the protein of interest within its physiologically relevant subcellular compartment in live cells (42). BRET is detected when energy emitted by the *Renilla* luciferase (Rluc) of a donor fusion protein is transferred to an acceptor YFP fusion partner following catalytic degradation of the cell-permeable Rluc substrate coelenterazine H (Fig. 7A) (14). In the first set of experiments, we performed DSA by using capsid proteins fused N terminally with either YFP or Rluc (Fig. 1A). As shown in Fig. 7A, a nonlinear increase in BRET intensity and a rapid saturation of the BRET signal was detected when a fixed amount of the Rluc-capsid construct was coexpressed with increasing quantities of the YFP-capsid construct. This pattern clearly indicated specific capsid self-interaction. In contrast, increasing concentrations of a

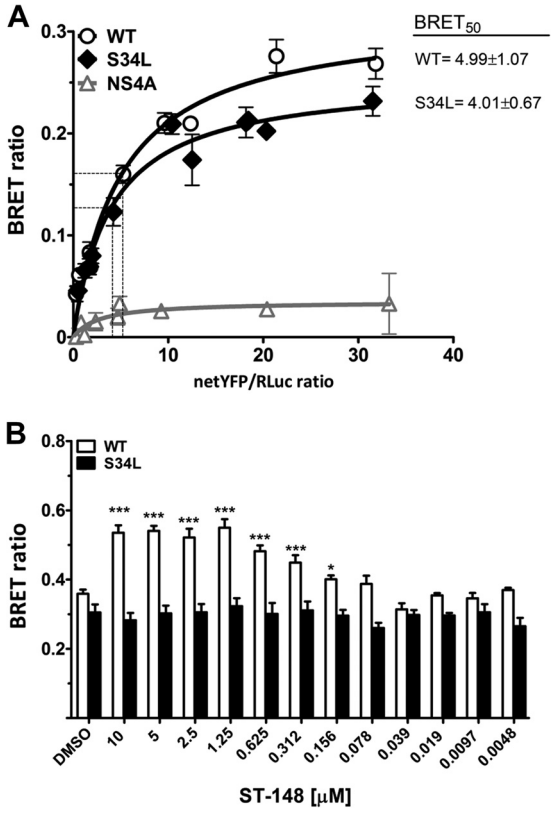

FIG 7 ST-148 increases DV capsid protein self-interaction. (A) Self-interaction kinetics of WT and S43L capsid as determined by BRET. DSA were performed in live 293T cells cotransfected with increasing amounts of YFP-tagged and a constant amount of Rluc-tagged plasmids encoding WT or mutant (S34L) capsid or NS4A, which served as negative controls. Forty-eight hours later, energy transfer was induced by the addition of the *Renilla* luciferase substrate coelenterazine H. The *x* axis shows the ratio between the normalized fluorescence of the acceptor (netYFP) measured before coelenterazine addition and the luminescence of the donor. $BRET_{50}$ values (netYFP/*Renilla* ratio at which 50% of maximal BRET is occurring), which reflect the relative affinity of the acceptor protein for the donor protein, are given in the top right of the panel. Curves represent the means ± standard deviations of results from one representative experiment carried out in triplicate. The curves were fitted using a nonlinear regression equation in which a single binding site was assumed. (B) Effect of ST-148 on capsid self interaction. 293T cells were transfected with 1 μg of YFP capsid and 20 ng of Rluc capsid (WT and S34L). Prior to transfection, different concentrations of ST-148 or DMSO were added to the medium, and 48 h later BRET was measured (***, $P < 0.001$; *, $P < 0.01$).

YFP-NS4A construct (used as a negative control) coexpressed with the Rluc-capsid construct resulted in only a weak and linear increase of BRET, which is a characteristic pattern for noninteracting proteins (43, 44).

Besides providing information on the specificity of a given interaction determined by BRET, additional parameters, such as $BRET_{max}$, i.e., the BRET signal at which the saturation curve reaches a plateau, and $BRET_{50}$, i.e., the concentration of acceptor giving 50% of $BRET_{max}$, can be extrapolated from DSA experiments. While $BRET_{max}$ is a function of the distance and orientation between the donor and acceptor within their oligomeric complex, $BRET_{50}$ reflects the relative affinity between the fusion proteins. As deduced from the $BRET_{50}$ values, the S34L mutation did not alter capsid self-interaction, and no significant difference between the oligomerization profiles of WT and S34L capsid proteins could be observed ($BRET_{50}$ of WT, 4.99 ± 1.071; $BRET_{50}$ of the S34L mutant, 4.01 ± 0.67) (Fig. 7A).

We next evaluated the effect of increasing concentrations of ST-148 on WT and S34L capsid self-interaction under conditions of $BRET_{max}$, i.e., ~50-fold excess of YFP-capsid plasmid relative to the Rluc-capsid plasmid (Fig. 7B). Under these conditions, we observed a dose-dependent increase of the BRET ratio, first detectable at 156 nM ST-148 and reaching a plateau at 1.25 μM. This increase in BRET signal was found only with the WT capsid protein, whereas the oligomerization status of the S34L capsid appeared unaffected for all tested concentrations, demonstrating the specificity of the ST-148-mediated enhancement of capsid self-interaction. These results support the notion that ST-148 directly affects capsid protein. The correlation between antiviral efficacy and enhancement of capsid self-interaction argues that increased capsid oligomerization is responsible for the antiviral activity of ST-148.

***In silico* modeling corroborates ST-148-mediated stabilization of interdimer capsid interactions.** To further understand the mode of action of ST-148 at the molecular level, we performed molecular modeling studies of WT and S34L capsid protein by using protein-protein docking, MD simulations, and small-molecule docking. These studies were based on the NMR structures reported by Ma et al. (PDB accession no. 1R6R) (12). Since capsid protein was reported to form stable dimers in solution (10, 12), they were considered fundamental units; therefore, the formation of tetramers was simulated. Since we observed the nuclear accumulation of capsid in the presence of ST-148, only tetramers that did not involve nuclear localization sequences (NLS) (28) at the interaction surfaces were considered, assuming that otherwise these NLS were hidden. Likewise, complexes that did not involve LD-binding domains (12, 45, 46) were preferred, because no effect on capsid-LD colocalization by ST-148 was detected. Priority was given to complexes in which the protein-protein interaction surface involved Ser34, as this amino acid residue was altered in the case of the ST-148-resistant DV mutant (Fig. 8A). The symmetry of the tetramer was not considered an important element, as cryo-electron microscopy data revealed that the DV nucleocapsid is disordered (47, 48, 49).

Two 30-ns MD simulations were performed on the best tetramer complex: one on the WT and one on the same structure containing the S34L mutation. In accordance with the BRET data, the two structures behaved similarly, indicating no differences between the WT and the mutant proteins in the absence of the inhibitor. In both cases, the tetramer quaternary structure changed during the first 2 ns (see Videos S1 and S2 in the supplemental material) and was stable for the rest of the simulation, suggesting that the system reaches equilibrium.

By using the energy-minimized tetramer structures of both the WT and S34L capsid, we next docked ST-148 using a 30-Å grid centered on the two Ser34 (or Leu34 in case of the mutant) residues at the dimer-dimer interface and examined the obtained ST-148 pose for WT and the S34L mutant over a 30-ns MD simulation. Comparable to the MD simulations in the absence of ligands, a similar change in the quaternary structures of both WT and S34L capsid could be observed during the first 2 ns (see Videos S3 and S4 in the supplemental material), and then the system reached equilibrium. Figure 8B shows the final MD result structures obtained for the WT protein in absence (left) or in the presence (right) of ST-148. In the case of the WT capsid, ST-148 bound the

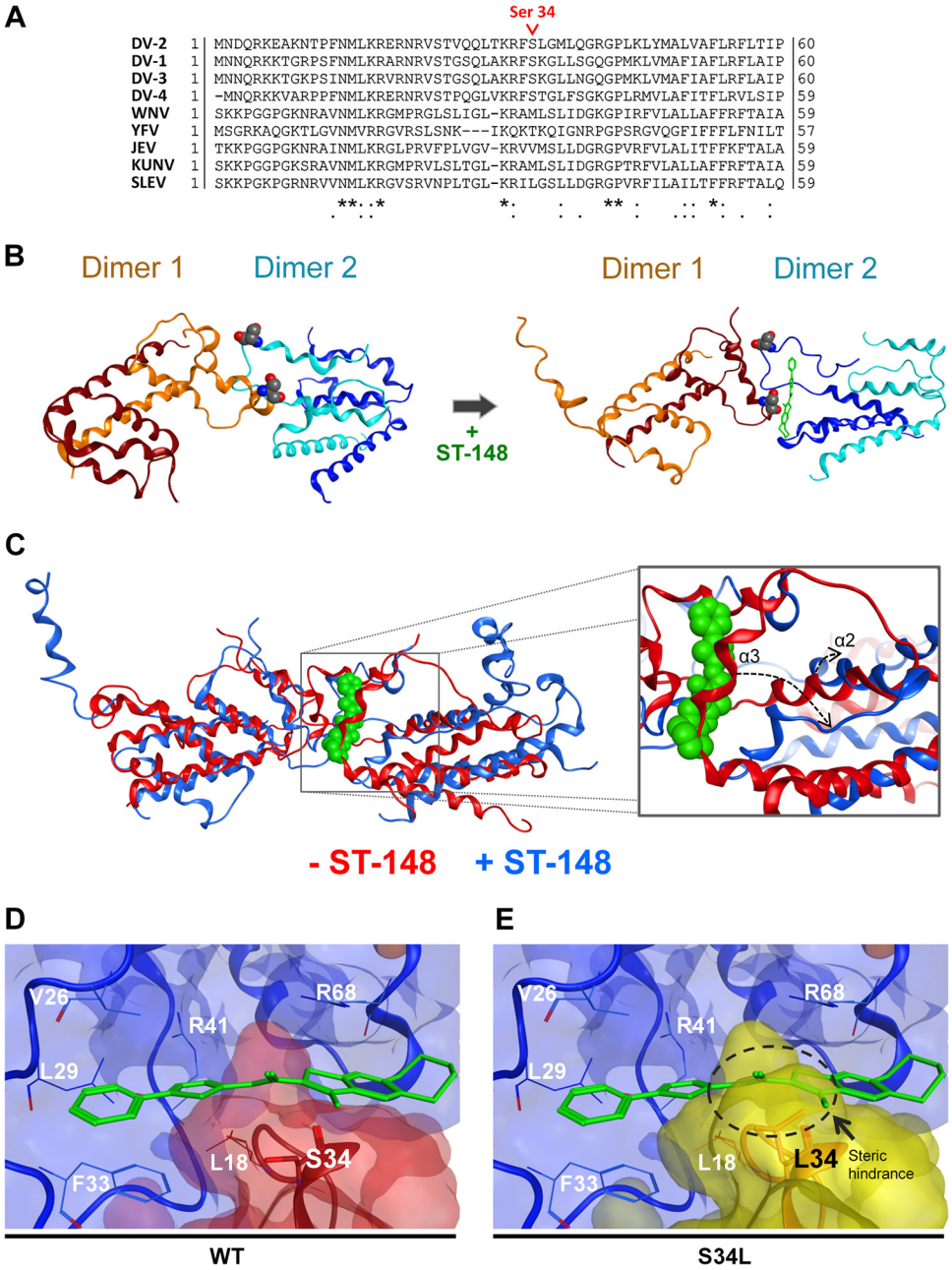

FIG 8 Docking model of ST-148 and DV capsid and possible stabilization of interdimer capsid protein interaction. (A) Sequence comparison of capsid amino acid sequences of DV serotypes 1 to 4 and selected flaviviruses. The position of serine 34 is highlighted in red. Sequence alignment was carried out using the ClustalW algorithm, available at the Uniprot webserver, on the following isolates: DV-2 (Thailand/16681-PDK53), DV-1 (Brazil/97-11/1997), DV-3 (Martinique/1243/1999), DV-4 (Thailand/0348/1991), West-Nile virus (WNV; H442), yellow fever virus (YFV; Ivory Coast/1999), Japanese encephalitis virus (JEV; SA-14), Kunjin virus (KUNV; MRM61C), and St. Louis encephalitis virus (SLEV; MS1-7). UniprotKB accession numbers are given in Materials and Methods. (B) Results from molecular dynamics (MD) simulations. Stable conformations of the WT capsid tetramer in the absence (left) or presence (right) of ST-148. Capsid dimers are represented in blue and orange, with each monomer given in different shades of the same color. ST-148 is shown with green sticks, and the serine residue at position 34 is represented with the Corey-Pauling-Koltun (CPK) model. Movies of the MD simulations are given in the supplemental material. (C) Results of superimposition of the MD simulation of the WT C tetramer in the absence (red ribbon) or presence (blue ribbon) of ST-148 are presented at the left. ST-148 is shown in green with the CPK model. A closer view of the same superimposition is presented in the right panel with the same color code. The dashed arrows indicate the structural rearrangements, which occur at α2 and α3 helices upon ST-148 binding and allow accommodating the ligand. (D and E) Close-up view of the docking pose of ST-148. (D) WT capsid dimer-dimer interface complexed with ST-148. (E) Same interface as that shown in panel D, with the serine residue superimposed on Leu34. The dashed circle highlights the steric hindrance induced by the leucine residue at position 34, clarifying how the mutation impedes this binding pose. In both panels one dimer is depicted in light blue, while the other capsid dimer is in red in the case of the WT or in yellow in the case of the S34L resistance mutant. Protein residues are displayed as lines, while Ser34 and Leu34 are drawn with stick representations.

complex in a cleft between the α1 helix of one dimer and α1 and α3 helices of the other dimer and remained stable at this site for the last 10 ns of the simulation (see Video S5 in the supplemental material). It is worth noting that ST-148 induced a shift of the α3 and α2 helices (Fig. 8C, dashed arrows), creating the ligand cleft and stabilizing further compound binding. Conversely, in the case of the S34L mutant protein, the compound did not bind a cleft at the dimer-dimer interface but explored more than one site in a solvent-exposed area of one dimer (see Video S6 in the supplemental material).

To confirm this difference in ligand binding between the two structures, we used the stable WT tetramer-ligand complex corresponding to the equilibrium state and docked ST-148 into the pocket identified during the MD by using a 20-Å grid (Fig. 8D). This docking confirmed that ST-148 is able to bind the tetramer at the dimer-dimer interface, and the same compound conformation obtained from the MD was reproduced. In the case of the WT structure, the binding site is formed primarily by residues Val26, Leu29, Arg41, and Arg68 of one dimer and Ser34 of the other dimer. As shown in Fig. 8D, the phenyl moiety of ST-148 binds Phe33 with a π-π stacking interaction, while the thieno[2,3-b] pyridine portion of ST-148 is tethered between Ser34 and Arg68, where the positive charge interacts with the electron-dense aromatic system. Furthermore, as ST-148 is highly lipophilic, its binding is enhanced by the large number of hydrophobic residues forming the pocket. As the compound is in close contact with Ser34, a leucine residue at this site creates a steric clash between the protein and the ligand (Fig. 8E), confirming that the S34L resistance mutation does not allow ST-148 to bind to the tetramer in the same way, consistent with the MD simulations. In summary, these results support the notion that ST-148 stabilizes capsid oligomerization and reveal a plausible model for compound binding to the capsid protein as well as binding inhibition by a distinct resistance mutation.

DISCUSSION

Capsid proteins of enveloped viruses have emerged as promising targets for the design of antiviral agents. In fact, the processes regulating both viral genome encapsidation and release during entry proved extremely sensitive to even subtle molecular disturbances (reviewed in reference 50). In this study, we describe the mechanism of action of ST-148, a recently identified small-molecule inhibitor that binds to and induces resistance in DV capsid (13). By using a combination of full-length reporter viruses and DV_{TCP}, we identified two distinct inhibitory effects: impaired DV entry and reduced production of infectious virus particles. Based on BRET assays, *in silico* docking, and MD simulations, we propose that these antiviral effects are the result of stabilized capsid self-interaction.

With respect to inhibition of virus entry, the lack of virucidal effects and the observed specific inhibitory effects of ST-148 on virus entry up to 30 min postinfection point toward a block in viral RNA uncoating. Although no detailed kinetics of nucleocapsid disassembly have been reported to date, earlier studies suggested that DV is internalized within 30 min after inoculation (51, 52). While our data do not demonstrate inhibition of the uncoating process, the observed increase of capsid self-interaction makes this assumption plausible. Nevertheless, additional experiments are required to directly demonstrate that viral RNA release is blocked at the nucleocapsid disassembly/RNA uncoating step.

In addition to impaired entry, ST-148 also reduced virus production. This might occur at the level of particle assembly or their release, but likely it is not due to alteration of specific infectivity of DV particles, as suggested by the concomitant reduction in both the released infectivity and the secreted viral RNA. Consistent with this result, we note that in spite of the overall reduction of electron-dense virus particles found within DV-infected cells upon ST-148 treatment, particle morphology appeared unaltered. Interestingly, these particles accumulated in larger numbers within ER stacks. Whether this phenomenon is a consequence of altered nucleocapsid assembly or results from disturbed intracellular transport of assembled virions remains to be determined. In any case, the observed redistribution of capsid from the cytosol to the nucleoli in ST-148-treated cells might contribute to the interference with virus production by reducing the amount of capsid protein available for assembly. Although lower cytoplasmic capsid levels also were observed for the DV^{S34L} mutant, its ability to traffic in and out of the nucleus likely is not compromised or is sufficient to support virion morphogenesis. Conversely, in the case of the WT capsid, the ST-148-induced nuclear retention correlated with an alteration of the protein (or protein complex) solubility, which might account for the observed reduction in virus production.

The proposed mechanism of action for both the early- and late-stage inhibition of ST-148 involves a direct effect on higher-order structures of DV capsid. This assumption is supported by the significant and dose-dependent increase in capsid self-interaction observed by BRET. Since we used conditions of $BRET_{max}$, our results suggest that the compound induces the formation of higher-order oligomeric capsid species or stabilizes further preexisting capsid dimers. This effect was specific for the WT capsid protein and not due to pleiotropic effects caused by the compound, because the interaction profile of the ST-148-resistant mutant was unaltered.

By using MD, we generated a model of a capsid tetramer in complex with ST-148. Obtained results confirmed that ST-148 stabilizes capsid self-interaction. Thus, ST-148 can be classified as a direct protein-protein interaction (PPI) stabilizer, establishing hydrophobic and electrostatic interactions in a cleft between the capsid dimers. As shown by our MD simulations, ST-148 retains the ability to bind the S34L-containing tetramer but in a less stable conformation and involving only one dimer. Therefore, molecular modeling data are in agreement with the previously observed binding of ST-148 to both the WT and the S34L-containing capsid protein (13). Furthermore, our *in silico* results clarify the role of S34L mutation in drug resistance, as the steric hindrance of leucine at position 34 impedes the stable binding of the compound to the tetrameric capsid protein complex.

Drug-induced modulation of capsid protein self-interactions is not unique to DV and has been described as an applicable strategy for several other enveloped viruses. For instance, in the case of hepatitis B virus (HBV), several inhibitors targeting the core protein have been reported, and at least two classes of HBV assembly effectors, the heteroaryldihydropyrimidines (HAPs) and phenylpropenamides, have been extensively characterized (53, 54, 55, 56). For the HAPs, elegant work from Zlotnick and colleagues demonstrated that these compounds can increase the kinetics of assembly and strengthen dimer-dimer association to stabilize capsids (57, 58). Comparable to HAPs, certain phenylpropenamides accelerate assembly and stabilize capsids, and some of these com-

pounds, such as AT-130, were shown to block viral RNA packaging without altering the geometry of nucleocapsids; they still formed, but they were devoid of nucleic acids (59, 60). Interestingly, molecules belonging to either class were shown to bind to partially overlapping sites of the HBV core protein.

In the case of HIV, different series of capsid inhibitors have been identified. For instance, the benzodiazepine (BD) and the benzimidazole (BM) series were reported to inhibit virion release or prevent virus maturation, respectively (61, 62). In the case of the BD series, molecular studies, complemented by nuclear magnetic resonance and crystallography approaches, have shown that compounds from this class inhibited HIV particle release by blocking assembly of immature capsids (63). Conversely, molecules of the BM series did not affect virus budding but prevented capsid maturation. Similar to HBV, these two compound series induced different biological phenotypes, although they both shared the same binding site within the N-terminal domain of the HIV capsid protein (64).

We note that Blair and colleagues characterized another series of HIV-1 capsid-targeting compounds interfering with both viral uncoating and formation of infectious particles (65). Similar to those of ST-148, these effects appeared to be mediated by the direct binding of the compound to HIV-1 capsid protein, increasing the rate of capsid protein multimerization. Similar to the study of Blair et al., a recent study reported the identification of a novel class of HIV-1 capsid inhibitors accelerating HIV capsid-nucleocapsid assembly and stabilizing preassembled capsid-nucleocapsid tubes against dissociation (66). These reports strengthen the concept of potent inhibition of viral replication via stabilization of the viral capsid.

Comparable to what has been reported for the anti-HBV HAPs, we hypothesize that the late-stage inhibitory effect of ST-148 on DV results from the stabilization of capsid protein interdimer association, which might reduce capsid plasticity and its ability to package viral RNA. Additionally, ST-148 seems to share selected features with the anti-HIV pyrrolopyrazolones, exerting antiviral activity on the early steps of the viral replication cycle, presumably by stabilizing preexisting capsid quaternary structures. However, the mechanism by which these HIV inhibitors stabilize capsid complexes is uncertain, because the inhibitor binding site does not reside within an inter- or intrahexameric capsid interface stabilizing the capsid lattice, while in case of ST-148, the putative binding site was identified between two DV capsid dimers.

A growing list of studies supports the notion that the multifunctional role of viral capsid protein, involving different protein conformations and interactions with different protein surfaces and host factors, represents a target that can be exploited for the development of potent inhibitors. Our work supports this hypothesis and argues that inhibitors targeting viral capsid proteins also are applicable to flaviviruses. Given the lack of approved DV-specific antiviral drugs, this target should be further investigated, ideally to design combination therapies with a high genetic resistance barrier.

In conclusion, we determined the mode of action of a DV capsid inhibitor that affects both entry and assembly/release of infectious virus particles. The antiviral effect appears to be mediated by enhanced capsid protein interaction, eventually inducing structural rigidity and/or steric hindrance during nucleocapsid formation. These results, together with the first description of a robust BRET-based assay to measure capsid self-interaction in live cells, might serve as a starting point for optimization of more effective therapeutics simultaneously targeting early and late stages of the DV life cycle.

ACKNOWLEDGMENTS

We thank Andrea Gamarnik and John G. Aaskov for the gift of rabbit polyclonal anti-C-specific and mouse monoclonal anti-C-specific antibodies, respectively. We are grateful to Martin Baril for insightful discussions on the BRET assay, Mirko Cortese for critical readings of the manuscript, and Wolfgang Fischl, Laurent Chatel-Chaix, and Stefan Seitz for helpful discussions.

This work was supported by grants from the European Union (Silver [grant no. 260644] and EUVIRNA [grant no. 264286]) and the Deutsche Forschungsgemeinschaft (SFB638, Teilprojekt A5), all to R.B.

When the study was initiated, C.M.B. and R.J. were employees of SIGA Technologies, Inc., and held stock in the company. R.J. no longer holds stock in SIGA.

REFERENCES

1. **Bhatt S, Gething PW, Brady OJ, Messina JP, Farlow AW, Moyes CL, Drake JM, Brownstein JS, Hoen AG, Sankoh O, Myers MF, George DB, Jaenisch T, Wint GR, Simmons CP, Scott TW, Farrar JJ, Hay SI.** 2013. The global distribution and burden of dengue. Nature **496:**504–507. http://dx.doi.org/10.1038/nature12060.
2. **Sabchareon A, Wallace D, Sirivichayakul C, Limkittikul K, Chanthavanich P, Suvannadabba S, Jiwariyavej V, Dulyachai W, Pengsaa K, Wartel TA, Moureau A, Saville M, Bouckenooghe A, Viviani S, Tornieporth NG, Lang J.** 2012. Protective efficacy of the recombinant, live-attenuated, CYD tetravalent dengue vaccine in Thai schoolchildren: a randomised, controlled phase 2b trial. Lancet **380:**1559–1567. http://dx.doi.org/10.1016/S0140-6736(12)61428-7.
3. **Nowak T, Farber PM, Wengler G, Wengler G.** 1989. Analyses of the terminal sequences of West Nile virus structural proteins and of the in vitro translation of these proteins allow the proposal of a complete scheme of the proteolytic cleavages involved in their synthesis. Virology **169:**365–376. http://dx.doi.org/10.1016/0042-6822(89)90162-1.
4. **Gollins SW, Porterfield JS.** 1986. The uncoating and infectivity of the flavivirus West Nile on interaction with cells: effects of pH and ammonium chloride. J. Gen. Virol. **67**(Part 9)**:**1941–1950. http://dx.doi.org/10.1099/0022-1317-67-9-1941.
5. **Heinz FX, Stiasny K, Puschner-Auer G, Holzmann H, Allison SL, Mandl CW, Kunz C.** 1994. Structural changes and functional control of the tick-borne encephalitis virus glycoprotein E by the heterodimeric association with protein prM. Virology **198:**109–117. http://dx.doi.org/10.1006/viro.1994.1013.
6. **Paul D, Bartenschlager R.** 2013. Architecture and biogenesis of plus-strand RNA virus replication factories. World J. Virol. **2:**32–48. http://dx.doi.org/10.5501/wjv.v2.i2.32.
7. **Belov GA, van Kuppeveld FJ.** 2012. (+)RNA viruses rewire cellular pathways to build replication organelles. Curr. Opin. Virol. **2:**740–747. http://dx.doi.org/10.1016/j.coviro.2012.09.006.
8. **Junjhon J, Pennington JG, Edwards TJ, Perera R, Lanman J, Kuhn RJ.** 2014. Ultrastructural characterization and three-dimensional architecture of replication sites in dengue virus-infected mosquito cells. J. Virol. **88:**4687–4697. http://dx.doi.org/10.1128/JVI.00118-14.
9. **Welsch S, Miller S, Romero-Brey I, Merz A, Bleck CK, Walther P, Fuller SD, Antony C, Krijnse-Locker J, Bartenschlager R.** 2009. Composition and three-dimensional architecture of the dengue virus replication and assembly sites. Cell Host Microbe **5:**365–375. http://dx.doi.org/10.1016/j.chom.2009.03.007.
10. **Jones CT, Ma L, Burgner JW, Groesch TD, Post CB, Kuhn RJ.** 2003. Flavivirus capsid is a dimeric alpha-helical protein. J. Virol. **77:**7143–7149. http://dx.doi.org/10.1128/JVI.77.12.7143-7149.2003.
11. **Wang SH, Syu WJ, Hu ST.** 2004. Identification of the homotypic interaction domain of the core protein of dengue virus type 2. J. Gen. Virol. **85:**2307–2314. http://dx.doi.org/10.1099/vir.0.80067-0.
12. **Ma L, Jones CT, Groesch TD, Kuhn RJ, Post CB.** 2004. Solution structure of dengue virus capsid protein reveals another fold. Proc. Natl.

Acad. Sci. U. S. A. **101:**3414–3419. http://dx.doi.org/10.1073/pnas.0305892101.
13. **Byrd CM, Dai D, Grosenbach DW, Berhanu A, Jones KF, Cardwell KB, Schneider C, Wineinger KA, Page JM, Harver C, Stavale E, Tyavanagimatt S, Stone MA, Bartenschlager R, Scaturro P, Hruby DE, Jordan R.** 2013. A novel inhibitor of dengue virus replication that targets the capsid protein. Antimicrob. Agents Chemother. **57:**15–25. http://dx.doi.org/10.1128/AAC.01429-12.
14. **Angers S, Salahpour A, Joly E, Hilairet S, Chelsky D, Dennis M, Bouvier M.** 2000. Detection of beta 2-adrenergic receptor dimerization in living cells using bioluminescence resonance energy transfer (BRET). Proc. Natl. Acad. Sci. U. S. A. **97:**3684–3689. http://dx.doi.org/10.1073/pnas.97.7.3684.
15. **Samsa MM, Mondotte JA, Iglesias NG, Assuncao-Miranda I, Barbosa-Lima G, Da Poian AT, Bozza PT, Gamarnik AV.** 2009. Dengue virus capsid protein usurps lipid droplets for viral particle formation. PLoS Pathog. **5:**e1000632. http://dx.doi.org/10.1371/journal.ppat.1000632.
16. **Steinmann E, Brohm C, Kallis S, Bartenschlager R, Pietschmann T.** 2008. Efficient trans-encapsidation of hepatitis C virus RNAs into infectious virus-like particles. J. Virol. **82:**7034–7046. http://dx.doi.org/10.1128/JVI.00118-08.
17. **Fischl W, Bartenschlager R.** 2013. High-throughput screening using dengue virus reporter genomes. Methods Mol. Biol. **1030:**205–219. http://dx.doi.org/10.1007/978-1-62703-484-5_17.
18. **Van Der Spoel D, Lindahl E, Hess B, Groenhof G, Mark AE, Berendsen HJ.** 2005. GROMACS: fast, flexible, and free. J. Comput. Chem. **26:**1701–1718. http://dx.doi.org/10.1002/jcc.20291.
19. **Kumar A, Buhler S, Selisko B, Davidson A, Mulder K, Canard B, Miller S, Bartenschlager R.** 2013. Nuclear localization of dengue virus nonstructural protein 5 does not strictly correlate with efficient viral RNA replication and inhibition of type I interferon signaling. J. Virol. **87:**4545–4557. http://dx.doi.org/10.1128/JVI.03083-12.
20. **Paul D, Romero-Brey I, Gouttenoire J, Stoitsova S, Krijnse-Locker J, Moradpour D, Bartenschlager R.** 2011. NS4B self-interaction through conserved C-terminal elements is required for the establishment of functional hepatitis C virus replication complexes. J. Virol. **85:**6963–6976. http://dx.doi.org/10.1128/JVI.00502-11.
21. **Westaway EG.** 1973. Proteins specified by group B togaviruses in mammalian cells during productive infections. Virology **51:**454–465. http://dx.doi.org/10.1016/0042-6822(73)90444-3.
22. **Kudelko M, Brault JB, Kwok K, Li MY, Pardigon N, Peiris JS, Bruzzone R, Despres P, Nal B, Wang PG.** 2012. Class II ADP-ribosylation factors are required for efficient secretion of dengue viruses. J. Biol. Chem. **287:**767–777. http://dx.doi.org/10.1074/jbc.M111.270579.
23. **Harvey TJ, Liu WJ, Wang XJ, Linedale R, Jacobs M, Davidson A, Le TT, Anraku I, Suhrbier A, Shi PY, Khromykh AA.** 2004. Tetracycline-inducible packaging cell line for production of flavivirus replicon particles. J. Virol. **78:**531–538. http://dx.doi.org/10.1128/JVI.78.1.531-538.2004.
24. **Khromykh AA, Kenney MT, Westaway EG.** 1998. Trans-complementation of flavivirus RNA polymerase gene NS5 by using Kunjin virus replicon-expressing BHK cells. J. Virol. **72:**7270–7279.
25. **Gehrke R, Ecker M, Aberle SW, Allison SL, Heinz FX, Mandl CW.** 2003. Incorporation of tick-borne encephalitis virus replicons into virus-like particles by a packaging cell line. J. Virol. **77:**8924–8933. http://dx.doi.org/10.1128/JVI.77.16.8924-8933.2003.
26. **Ansarah-Sobrinho C, Nelson S, Jost CA, Whitehead SS, Pierson TC.** 2008. Temperature-dependent production of pseudoinfectious dengue reporter virus particles by complementation. Virology **381:**67-74. http://dx.doi.org/10.1016/j.virol.2008.08.021.
27. **Scholle F, Girard YA, Zhao Q, Higgs S, Mason PW.** 2004. Trans-packaged West Nile virus-like particles: infectious properties in vitro and in infected mosquito vectors. J. Virol. **78:**11605–11614. http://dx.doi.org/10.1128/JVI.78.21.11605-11614.2004.
28. **Sangiambut S, Keelapang P, Aaskov J, Puttikhunt C, Kasinrerk W, Malasit P, Sittisombut N.** 2008. Multiple regions in dengue virus capsid protein contribute to nuclear localization during virus infection. J. Gen. Virol. **89:**1254–1264. http://dx.doi.org/10.1099/vir.0.83264-0.
29. **Wang SH, Syu WJ, Huang KJ, Lei HY, Yao CW, King CC, Hu ST.** 2002. Intracellular localization and determination of a nuclear localization signal of the core protein of dengue virus. J. Gen. Virol. **83:**3093–3102.
30. **Westaway EG, Khromykh AA, Kenney MT, Mackenzie JM, Jones MK.** 1997. Proteins C and NS4B of the flavivirus Kunjin translocate independently into the nucleus. Virology **234:**31–41. http://dx.doi.org/10.1006/viro.1997.8629.
31. **Westaway EG, Mackenzie JM, Khromykh AA.** 2002. Replication and gene function in Kunjin virus. Curr. Top. Microbiol. Immunol. **267:**323–351. http://dx.doi.org/10.1007/978-3-642-59403-8_16.
32. **Mackenzie JM, Westaway EG.** 2001. Assembly and maturation of the flavivirus Kunjin virus appear to occur in the rough endoplasmic reticulum and along the secretory pathway, respectively. J. Virol. **75:**10787–10799. http://dx.doi.org/10.1128/JVI.75.22.10787-10799.2001.
33. **Bhuvanakantham R, Cheong YK, Ng ML.** 2010. West Nile virus capsid protein interaction with importin and HDM2 protein is regulated by protein kinase C-mediated phosphorylation. Microbes Infect. **12:**615–625. http://dx.doi.org/10.1016/j.micinf.2010.04.005.
34. **Balinsky CA, Schmeisser H, Ganesan S, Singh K, Pierson TC, Zoon KC.** 2013. Nucleolin interacts with the dengue virus capsid protein and plays a role in formation of infectious virus particles. J. Virol. **87:**13094–13106. http://dx.doi.org/10.1128/JVI.00704-13.
35. **Xu Z, Anderson R, Hobman TC.** 2011. The capsid-binding nucleolar helicase DDX56 is important for infectivity of West Nile virus. J. Virol. **85:**5571–5580. http://dx.doi.org/10.1128/JVI.01933-10.
36. **Cheong YK, Ng ML.** 2011. Dephosphorylation of West Nile virus capsid protein enhances the processes of nucleocapsid assembly. Microbes Infect. **13:**76–84. http://dx.doi.org/10.1016/j.micinf.2010.10.014.
37. **Mori Y, Okabayashi T, Yamashita T, Zhao Z, Wakita T, Yasui K, Hasebe F, Tadano M, Konishi E, Moriishi K, Matsuura Y.** 2005. Nuclear localization of Japanese encephalitis virus core protein enhances viral replication. J. Virol. **79:**3448–3458. http://dx.doi.org/10.1128/JVI.79.6.3448-3458.2005.
38. **Bulich R, Aaskov JG.** 1992. Nuclear localization of dengue 2 virus core protein detected with monoclonal antibodies. J. Gen. Virol. **73**(Part 11)**:**2999–3003. http://dx.doi.org/10.1099/0022-1317-73-11-2999.
39. **Netsawang J, Noisakran S, Puttikhunt C, Kasinrerk W, Wongwiwat W, Malasit P, Yenchitsomanus PT, Limjindaporn T.** 2010. Nuclear localization of dengue virus capsid protein is required for DAXX interaction and apoptosis. Virus Res. **147:**275–283. http://dx.doi.org/10.1016/j.virusres.2009.11.012.
40. **Chang CJ, Luh HW, Wang SH, Lin HJ, Lee SC, Hu ST.** 2001. The heterogeneous nuclear ribonucleoprotein K (hnRNP K) interacts with dengue virus core protein. DNA Cell Biol. **20:**569–577. http://dx.doi.org/10.1089/104454901317094981.
41. **Colpitts TM, Barthel S, Wang P, Fikrig E.** 2011. Dengue virus capsid protein binds core histones and inhibits nucleosome formation in human liver cells. PLoS One **6:**e24365. http://dx.doi.org/10.1371/journal.pone.0024365.
42. **Pfleger KD, Seeber RM, Eidne KA.** 2006. Bioluminescence resonance energy transfer (BRET) for the real-time detection of protein-protein interactions. Nat. Protoc. **1:**337–345. http://dx.doi.org/10.1038/nprot.2006.52.
43. **Baril M, Racine ME, Penin F, Lamarre D.** 2009. MAVS dimer is a crucial signaling component of innate immunity and the target of hepatitis C virus NS3/4A protease. J. Virol. **83:**1299–1311. http://dx.doi.org/10.1128/JVI.01659-08.
44. **Mercier JF, Salahpour A, Angers S, Breit A, Bouvier M.** 2002. Quantitative assessment of beta 1- and beta 2-adrenergic receptor homo- and heterodimerization by bioluminescence resonance energy transfer. J. Biol. Chem. **277:**44925–44931. http://dx.doi.org/10.1074/jbc.M205767200.
45. **Markoff L, Falgout B, Chang A.** 1997. A conserved internal hydrophobic domain mediates the stable membrane integration of the dengue virus capsid protein. Virology **233:**105–117. http://dx.doi.org/10.1006/viro.1997.8608.
46. **Martins IC, Gomes-Neto F, Faustino AF, Carvalho FA, Carneiro FA, Bozza PT, Mohana-Borges R, Castanho MA, Almeida FC, Santos NC, Da Poian AT.** 2012. The disordered N-terminal region of dengue virus capsid protein contains a lipid-droplet-binding motif. Biochem. J. **444:**405–415. http://dx.doi.org/10.1042/BJ20112219.
47. **Kuhn RJ, Zhang W, Rossmann MG, Pletnev SV, Corver J, Lenches E, Jones CT, Mukhopadhyay S, Chipman PR, Strauss EG, Baker TS, Strauss JH.** 2002. Structure of dengue virus: implications for flavivirus organization, maturation, and fusion. Cell **108:**717–725. http://dx.doi.org/10.1016/S0092-8674(02)00660-8.
48. **Zhang W, Chipman PR, Corver J, Johnson PR, Zhang Y, Mukhopadhyay S, Baker TS, Strauss JH, Rossmann MG, Kuhn RJ.** 2003. Visualization of membrane protein domains by cryo-electron microscopy of

dengue virus. Nat. Struct. Biol. **10:**907–912. http://dx.doi.org/10.1038/nsb990.

49. **Zhang X, Ge P, Yu X, Brannan JM, Bi G, Zhang Q, Schein S, Zhou ZH.** 2013. Cryo-EM structure of the mature dengue virus at 3.5-A resolution. Nat. Struct. Mol. Biol. **20:**105–110. http://dx.doi.org/10.1038/nsmb.2463.
50. **Klumpp K, Crepin T.** 2014. Capsid proteins of enveloped viruses as antiviral drug targets. Curr. Opin. Virol. **5C:**63–71. http://dx.doi.org/10.1016/j.coviro.2014.02.002.
51. **Acosta EG, Castilla V, Damonte EB.** 2012. Differential requirements in endocytic trafficking for penetration of dengue virus. PLoS One **7:**e44835. http://dx.doi.org/10.1371/journal.pone.0044835.
52. **van der Schaar HM, Rust MJ, Chen C, Ende-Metselaar H, Wilschut J, Zhuang X, Smit JM.** 2008. Dissecting the cell entry pathway of dengue virus by single-particle tracking in living cells. PLoS Pathog. **4:**e1000244. http://dx.doi.org/10.1371/journal.ppat.1000244.
53. **Delaney WE, Edwards R, Colledge D, Shaw T, Furman P, Painter G, Locarnini S.** 2002. Phenylpropenamide derivatives AT-61 and AT-130 inhibit replication of wild-type and lamivudine-resistant strains of hepatitis B virus in vitro. Antimicrob. Agents Chemother. **46:**3057–3060. http://dx.doi.org/10.1128/AAC.46.9.3057-3060.2002.
54. **Deres K, Schroder CH, Paessens A, Goldmann S, Hacker HJ, Weber O, Kramer T, Niewohner U, Pleiss U, Stoltefuss J, Graef E, Koletzki D, Masantschek RN, Reimann A, Jaeger R, Gross R, Beckermann B, Schlemmer KH, Haebich D, Rubsamen-Waigmann H.** 2003. Inhibition of hepatitis B virus replication by drug-induced depletion of nucleocapsids. Science **299:**893–896. http://dx.doi.org/10.1126/science.1077215.
55. **King RW, Ladner SK, Miller TJ, Zaifert K, Perni RB, Conway SC, Otto MJ.** 1998. Inhibition of human hepatitis B virus replication by AT-61, a phenylpropenamide derivative, alone and in combination with (−)beta-L-2′,3′-dideoxy-3′-thiacytidine. Antimicrob. Agents Chemother. **42:**3179–3186.
56. **Perni RB, Conway SC, Ladner SK, Zaifert K, Otto MJ, King RW.** 2000. Phenylpropenamide derivatives as inhibitors of hepatitis B virus replication. Bioorg. Med. Chem. Lett. **10:**2687–2690. http://dx.doi.org/10.1016/S0960-894X(00)00544-8.
57. **Stray SJ, Bourne CR, Punna S, Lewis WG, Finn MG, Zlotnick A.** 2005. A heteroaryldihydropyrimidine activates and can misdirect hepatitis B virus capsid assembly. Proc. Natl. Acad. Sci. U. S. A. **102:**8138–8143. http://dx.doi.org/10.1073/pnas.0409732102.
58. **Zlotnick A, Ceres P, Singh S, Johnson JM.** 2002. A small molecule inhibits and misdirects assembly of hepatitis B virus capsids. J. Virol. **76:**4848–4854. http://dx.doi.org/10.1128/JVI.76.10.4848-4854.2002.
59. **Feld JJ, Colledge D, Sozzi V, Edwards R, Littlejohn M, Locarnini SA.** 2007. The phenylpropenamide derivative AT-130 blocks HBV replication at the level of viral RNA packaging. Antiviral Res. **76:**168–177. http://dx.doi.org/10.1016/j.antiviral.2007.06.014.
60. **Katen SP, Chirapu SR, Finn MG, Zlotnick A.** 2010. Trapping of hepatitis B virus capsid assembly intermediates by phenylpropenamide assembly accelerators. ACS Chem. Biol. **5:**1125–1136. http://dx.doi.org/10.1021/cb100275b.
61. **Fader LD, Bethell R, Bonneau P, Bos M, Bousquet Y, Cordingley MG, Coulombe R, Deroy P, Faucher AM, Gagnon A, Goudreau N, Grand-Maitre C, Guse I, Hucke O, Kawai SH, Lacoste JE, Landry S, Lemke CT, Malenfant E, Mason S, Morin S, O'Meara J, Simoneau B, Titolo S, Yoakim C.** 2011. Discovery of a 1,5-dihydrobenzo[1,4]diazepine-2,4-dione series of inhibitors of HIV-1 capsid assembly. Bioorg. Med. Chem. Lett. **21:**398–404. http://dx.doi.org/10.1016/j.bmcl.2010.10.131.
62. **Tremblay M, Bonneau P, Bousquet Y, Deroy P, Duan J, Duplessis M, Gagnon A, Garneau M, Goudreau N, Guse I, Hucke O, Kawai SH, Lemke CT, Mason SW, Simoneau B, Surprenant S, Titolo S, Yoakim C.** 2012. Inhibition of HIV-1 capsid assembly: optimization of the antiviral potency by site selective modifications at N1, C2 and C16 of a 5-(5-furan-2-yl-pyrazol-1-yl)-1H-benzimidazole scaffold. Bioorg. Med. Chem. Lett. **22:**7512–7517. http://dx.doi.org/10.1016/j.bmcl.2012.10.034.
63. **Goudreau N, Lemke CT, Faucher AM, Grand-Maitre C, Goulet S, Lacoste JE, Rancourt J, Malenfant E, Mercier JF, Titolo S, Mason SW.** 2013. Novel inhibitor binding site discovery on HIV-1 capsid N-terminal domain by NMR and X-ray crystallography. ACS Chem. Biol. **8:**1074–1082. http://dx.doi.org/10.1021/cb400075f.
64. **Lemke CT, Titolo S, von Schwedler U, Goudreau N, Mercier JF, Wardrop E, Faucher AM, Coulombe R, Banik SS, Fader L, Gagnon A, Kawai SH, Rancourt J, Tremblay M, Yoakim C, Simoneau B, Archambault J, Sundquist WI, Mason SW.** 2012. Distinct effects of two HIV-1 capsid assembly inhibitor families that bind the same site within the N-terminal domain of the viral CA protein. J. Virol. **86:**6643–6655. http://dx.doi.org/10.1128/JVI.00493-12.
65. **Blair WS, Pickford C, Irving SL, Brown DG, Anderson M, Bazin R, Cao J, Ciaramella G, Isaacson J, Jackson L, Hunt R, Kjerrstrom A, Nieman JA, Patick AK, Perros M, Scott AD, Whitby K, Wu H, Butler SL.** 2010. HIV capsid is a tractable target for small molecule therapeutic intervention. PLoS Pathog. **6:**e1001220. http://dx.doi.org/10.1371/journal.ppat.1001220.
66. **Lamorte L, Titolo S, Lemke CT, Goudreau N, Mercier JF, Wardrop E, Shah VB, von Schwedler UK, Langelier C, Banik SS, Aiken C, Sundquist WI, Mason SW.** 2013. Discovery of novel small-molecule HIV-1 replication inhibitors that stabilize capsid complexes. Antimicrob. Agents Chemother. **57:**4622–4631. http://dx.doi.org/10.1128/AAC.00985-13.